

Geophysical applications of nuclear resonant scattering

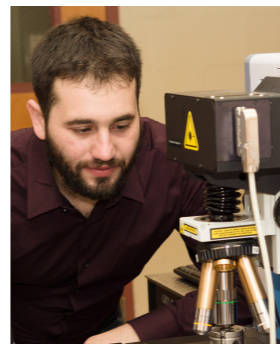


Jennifer M. Jackson

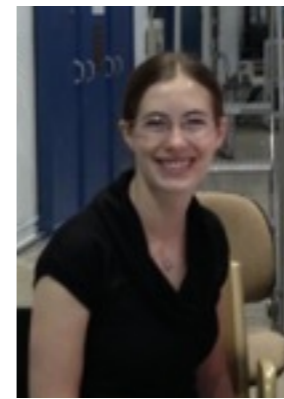
*Seismological Laboratory
Geological & Planetary Sciences
Caltech*

Workshop on Nuclear Resonant Scattering
Advanced Photon Source, Argonne National Laboratory
12 November 2016

Acknowledgements



Greg Finkelstein
SeismoLab Director's
Postdoctoral Fellow



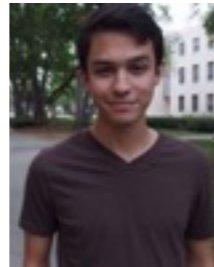
Rachel Morrison
Graduate Student



Natalia Solomatova
Graduate Student



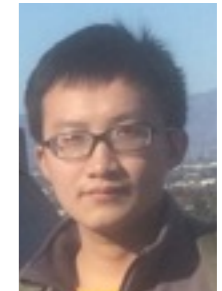
Wolfgang Sturhahn
Visiting Associate



Tyler Perez
Ayya Alieva
Undergraduate
Students



Vasilije Dobrosavljevic
Graduate Student



Maoyi Mao
Graduate Student

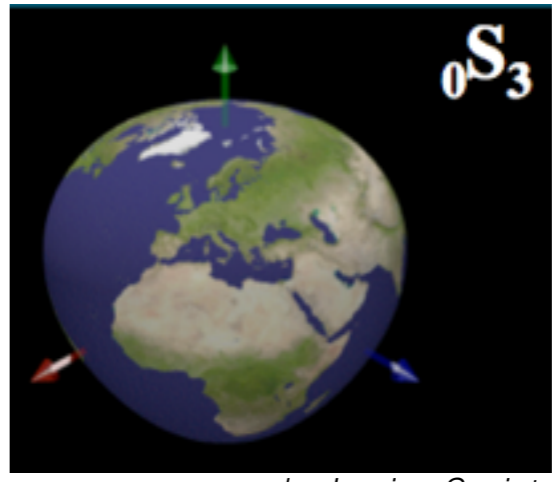
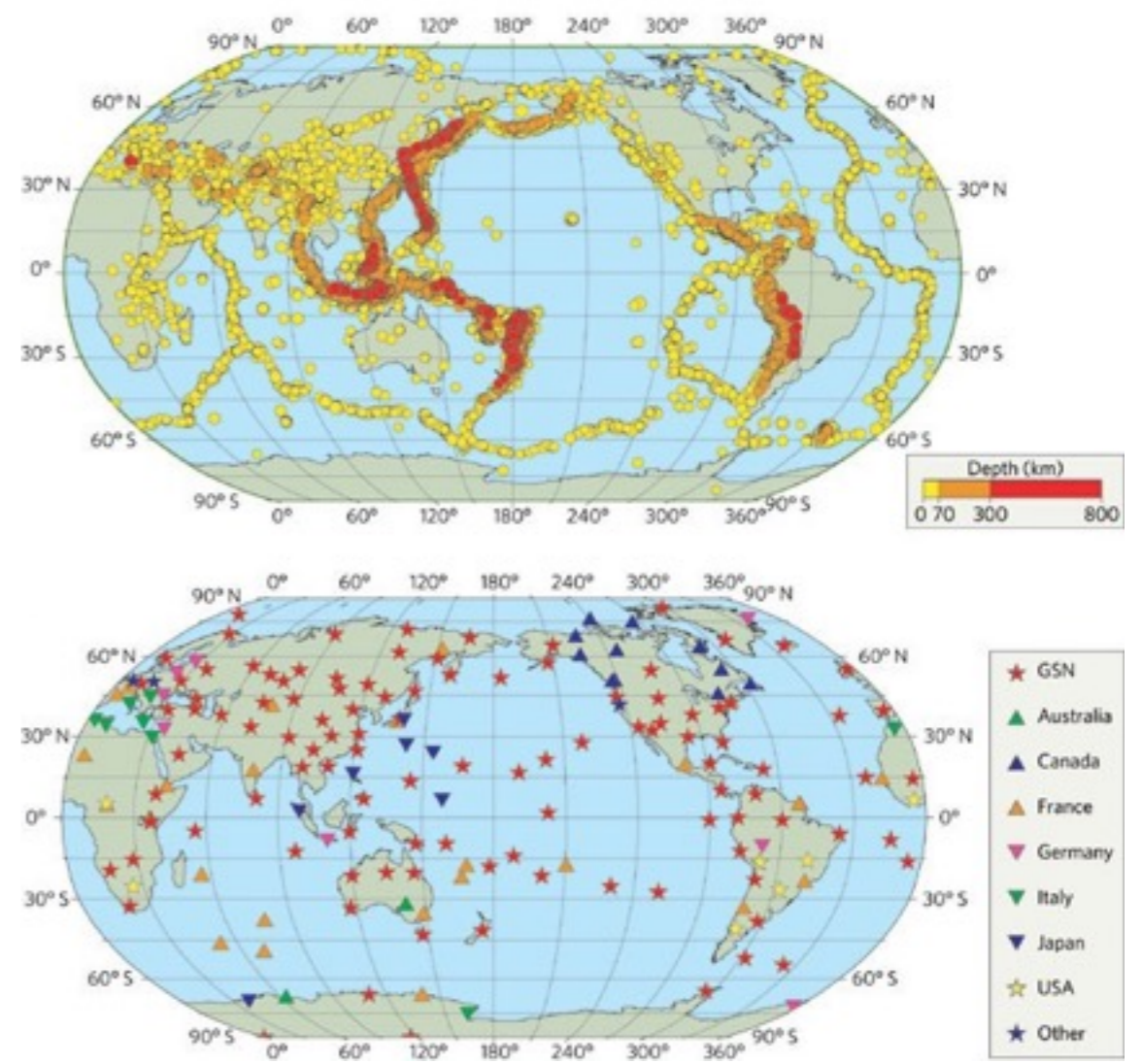
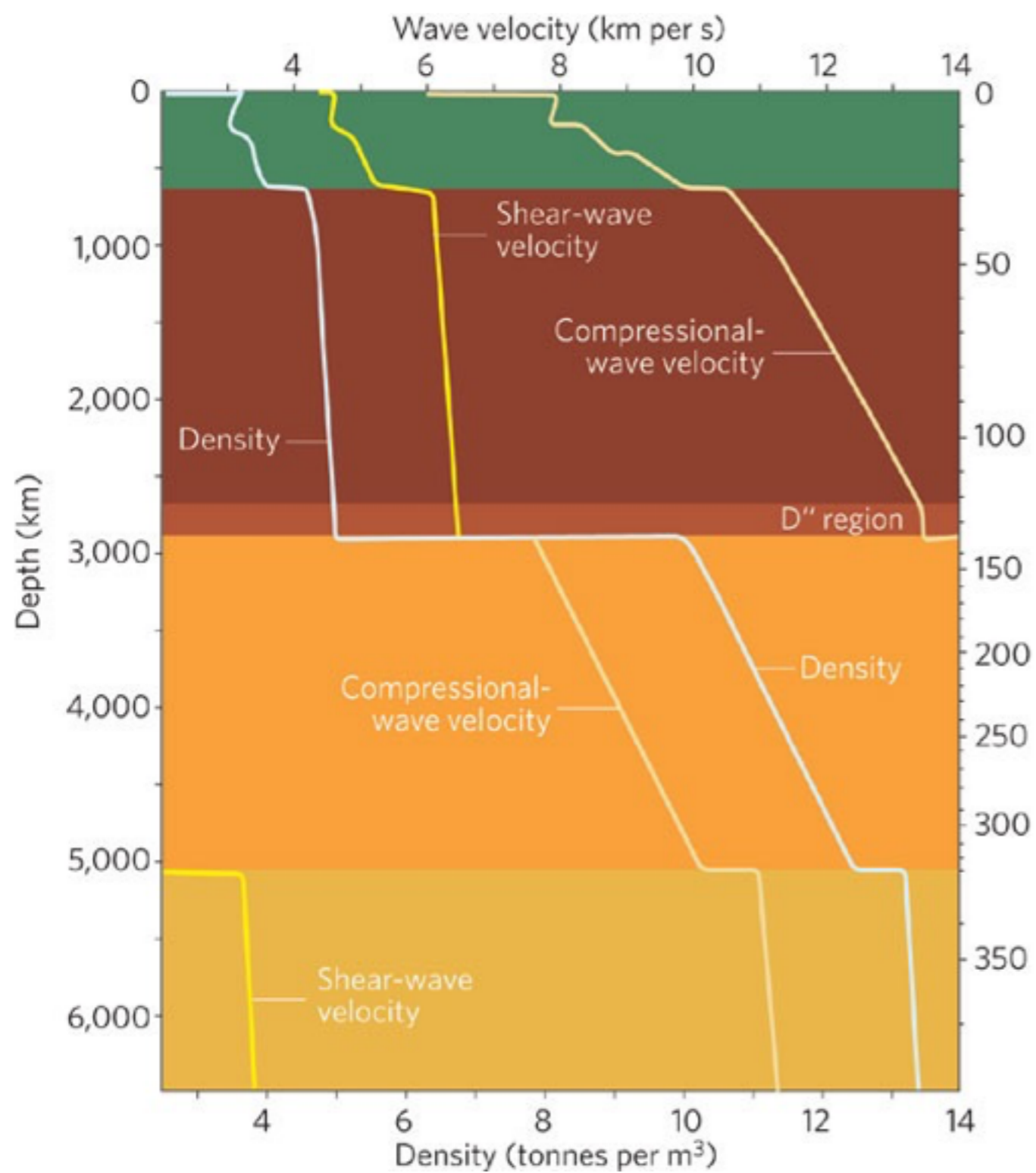
Dan Bower: now Postdoctoral Fellow at ETH, Zurich
Bin Chen: now Asst. Professor, Univ. of Hawaii
Caitlin Murphy: now Congressional Fellow, Washington DC
Daoyuan Sun: now Professor, Univ. Sci. Tech. China
June Wicks: now Assoc. Research Scholar, Princeton University
Aaron Wolf: now Asst. Research Scientist, Univ. of Michigan
Dongzhou Zhang: now Beamline Scientist, GSECARS/Univ. HI

Advanced Photon Source

Ercan Alp, Tom Toellner, Jiyong Zhao, Wenli Bi, Michael Hu (NRS)
Mark Rivers, Vitali Prakapenka (GSECARS)
Guoyin Shen (HP-CAT)



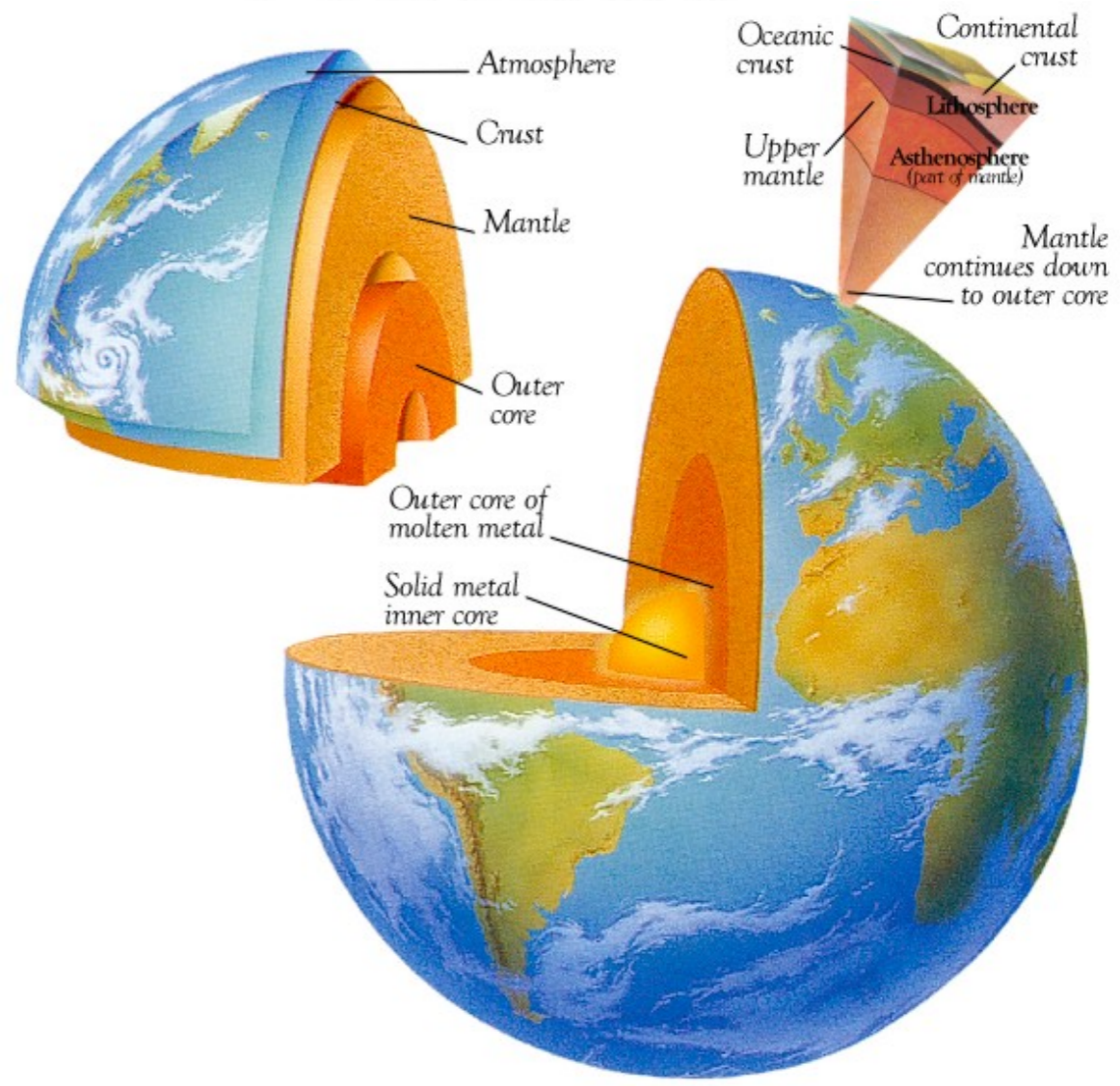
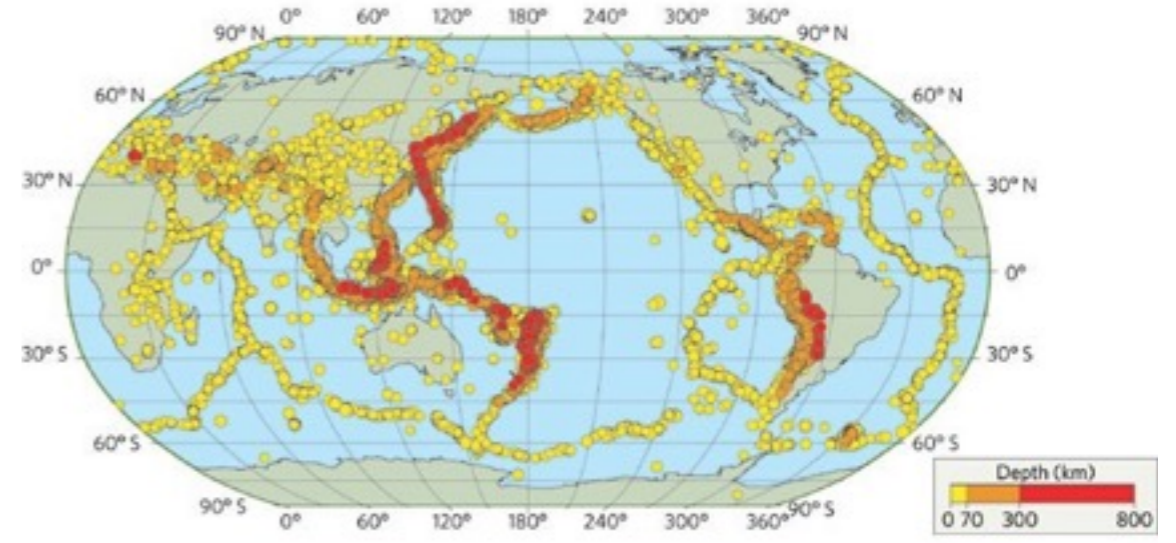
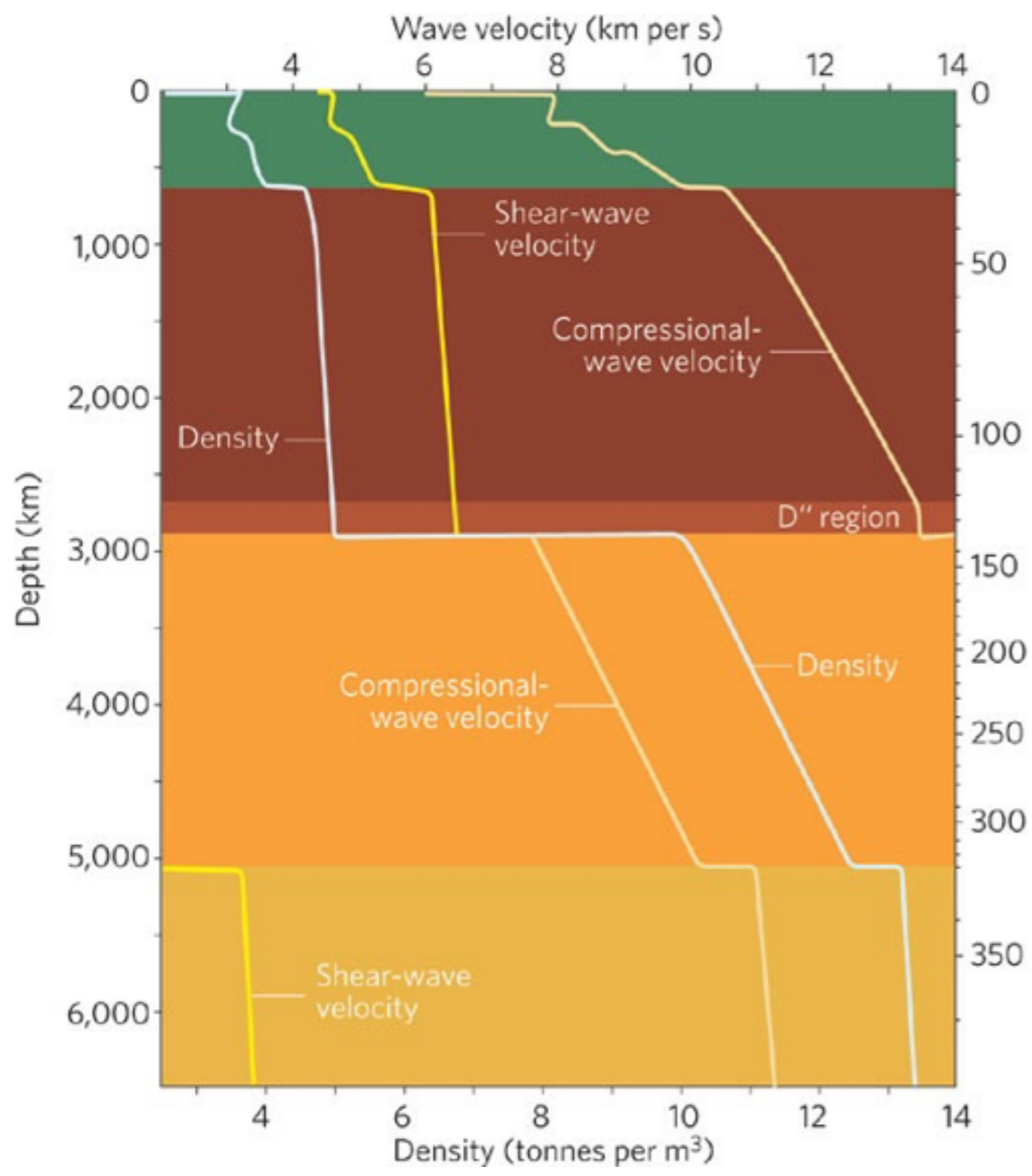
The first-order structure of Earth's interior



by Lucien Saviot



The first-order structure of Earth's interior

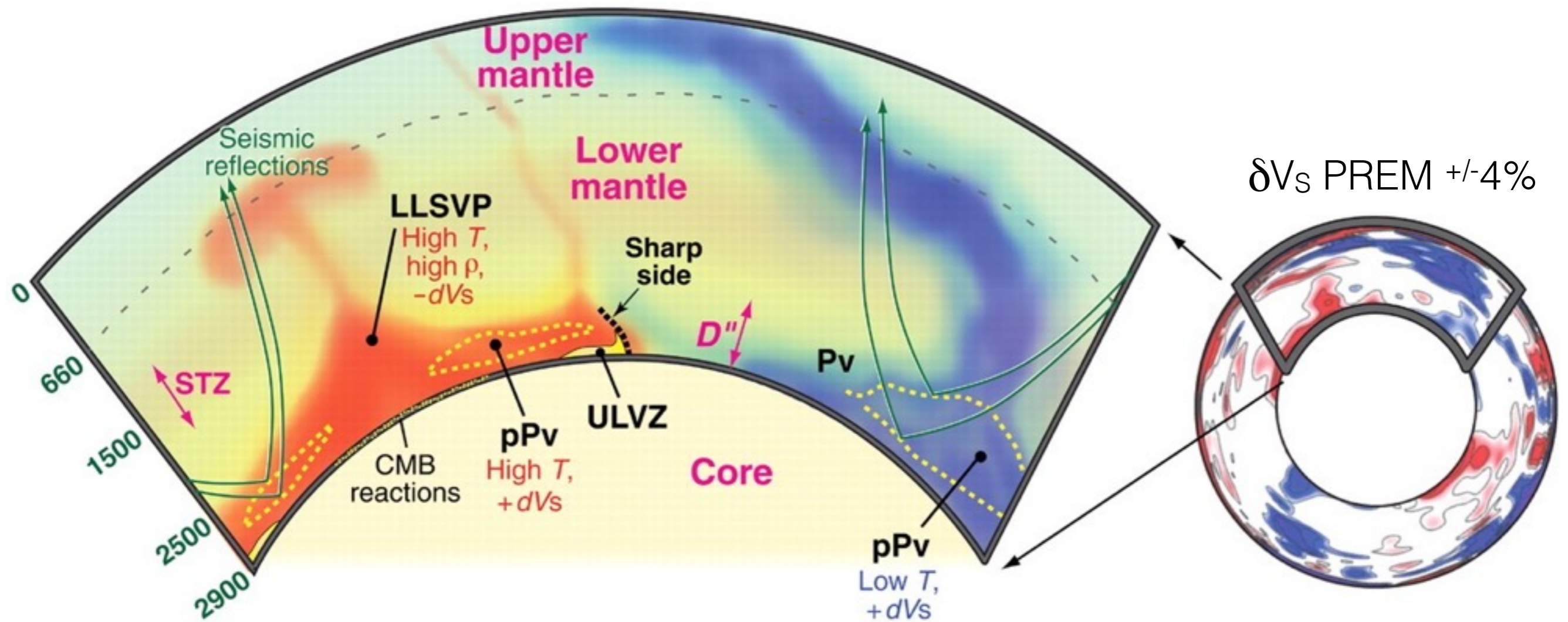


Preliminary Reference Earth Model (PREM): Dziewonski & Anderson (1981)
 Romanowicz, Nature (2008), Discovery Channel

Jennifer M. Jackson



Perturbations from the 1D model reveal multi-scale features



Sound velocities
Thermal expansion
Thermal pressure
Grüneisen parameter

Nuclear resonant inelastic x-ray scattering

Oxidation and spin states of iron
Magnetic ordering
Melting

Synchrotron Mössbauer spectroscopy

Minerals in a peridotitic mantle

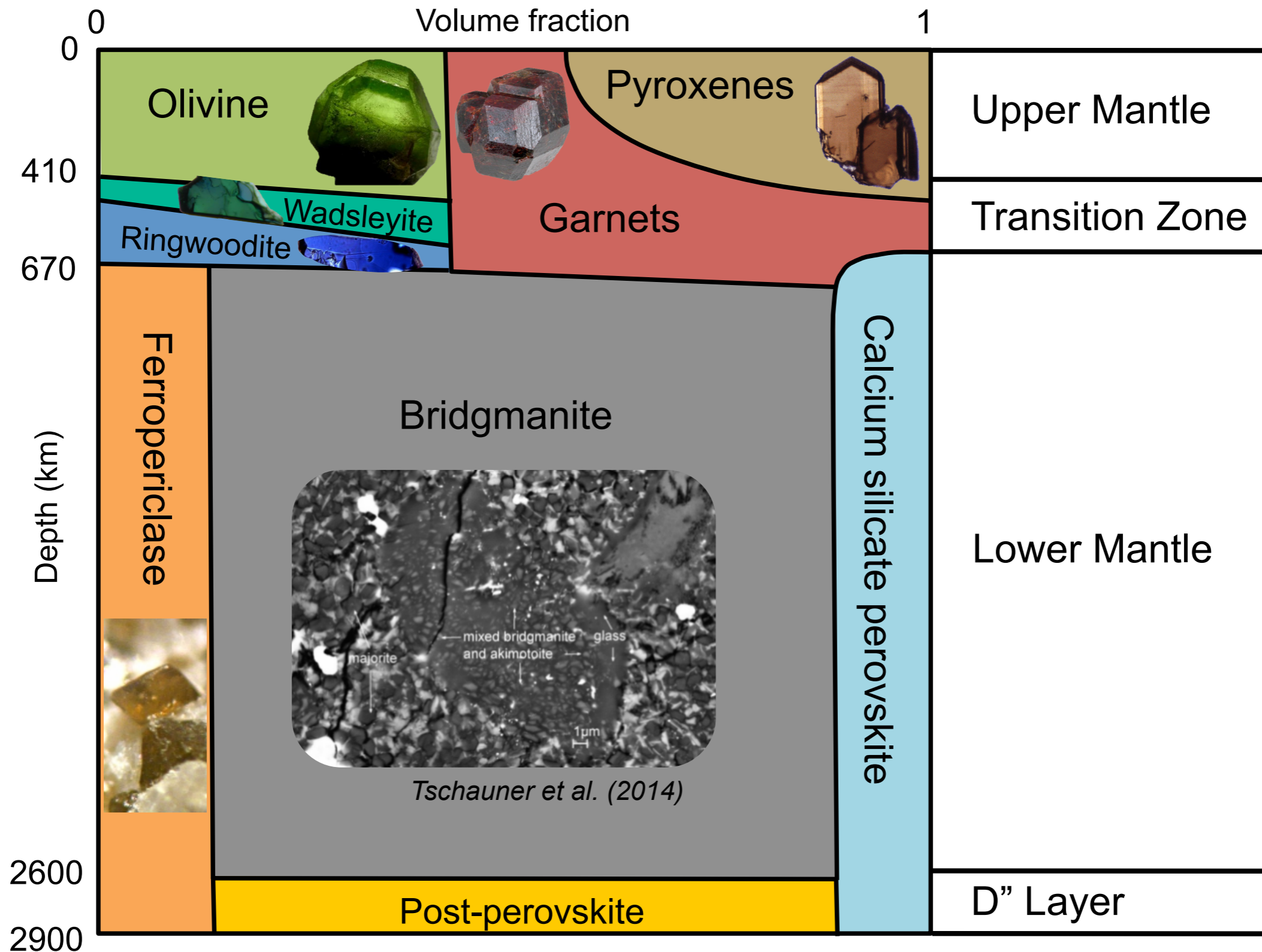
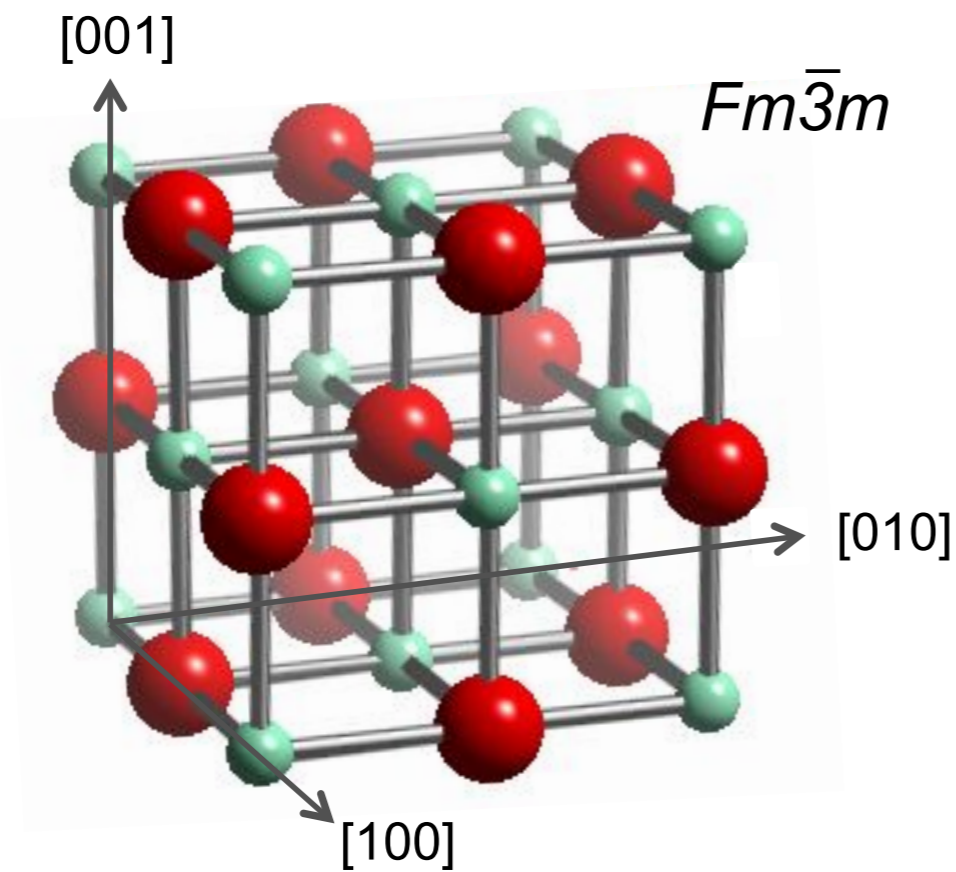
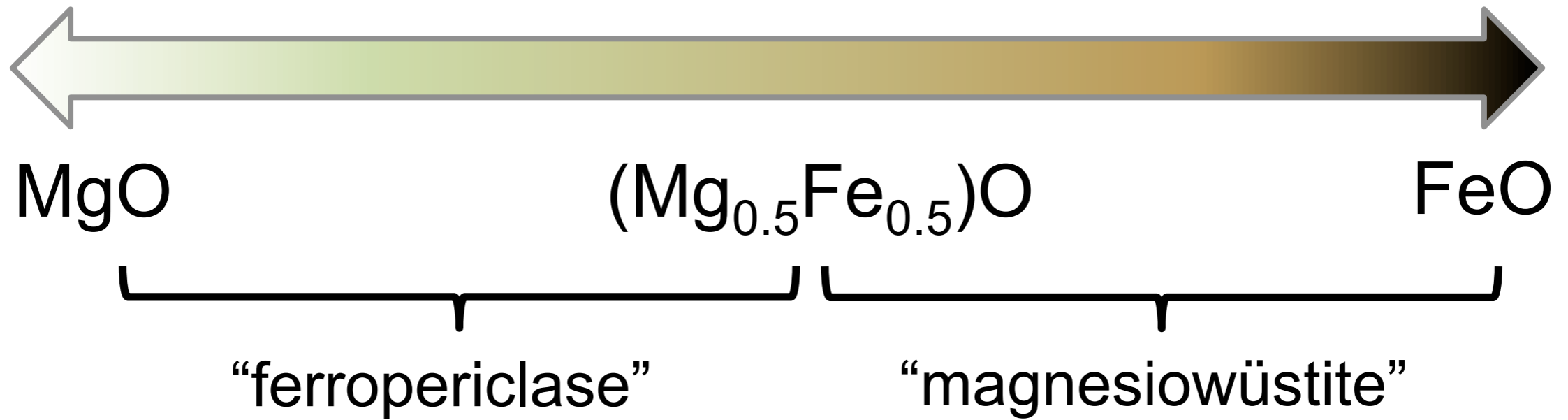
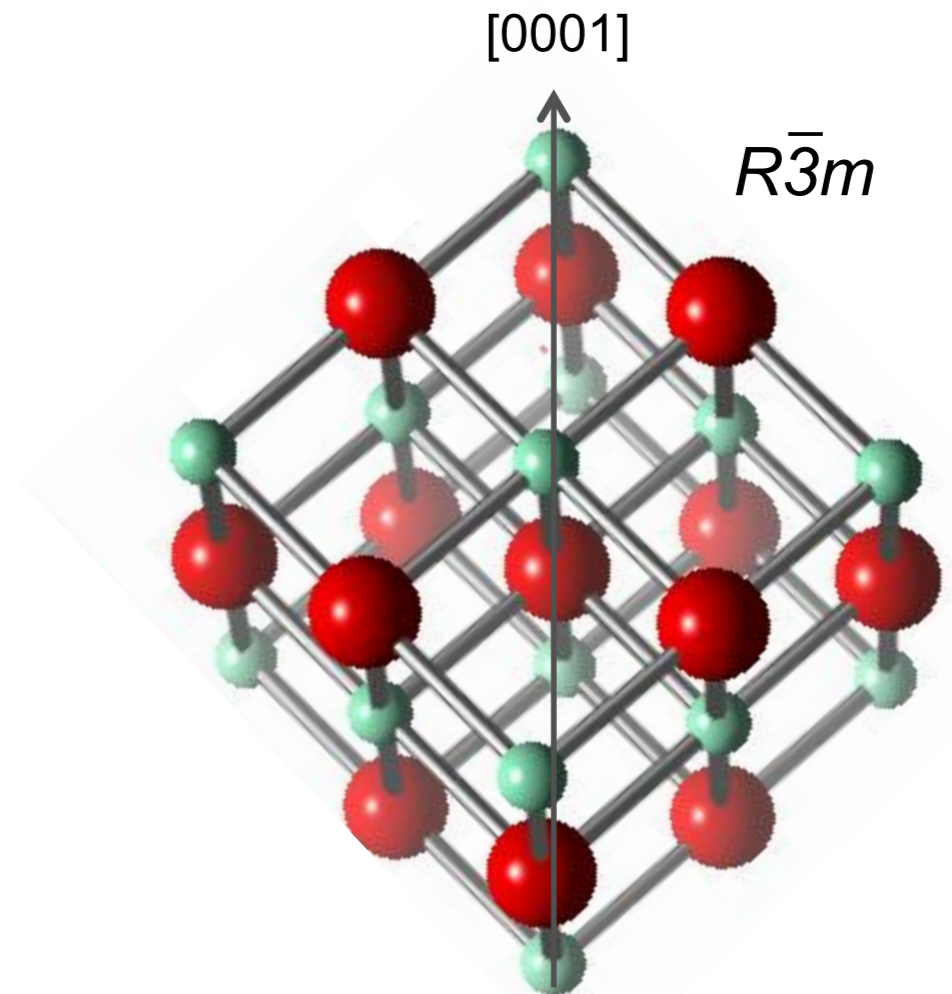


Figure created by Natalia Solomatova. After J. Amodeo; OPX from minerals.gps.caltech.edu; olivine by Rob Lavinsky; wadsleyite by T. Kawazoe; ringwoodite by Joe Smyth

Periclase - Wüstite Solid Solution

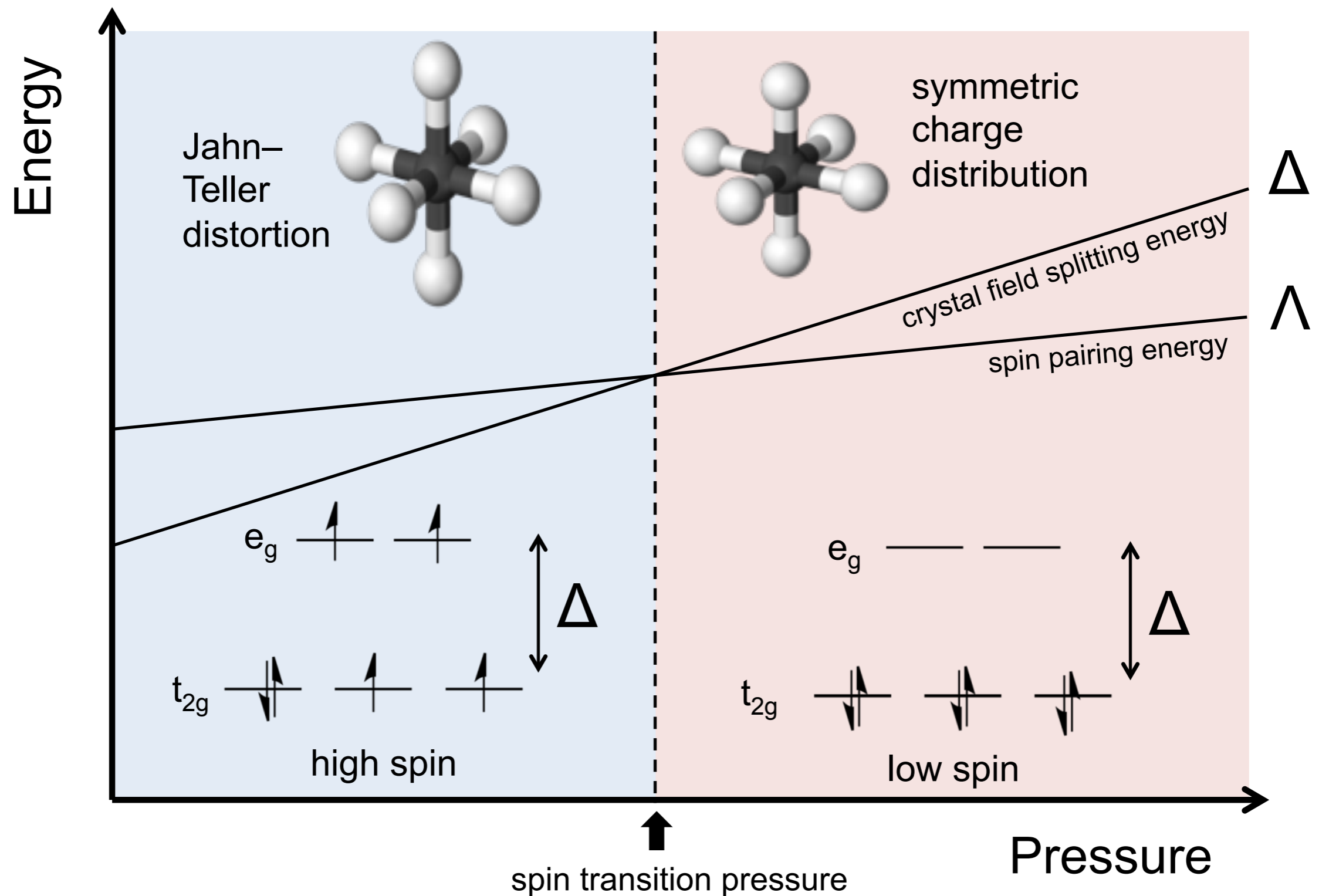


B1 phase




rhombohedral phase

Electronic spin pairing in octahedral ferrous iron



Previous Experiments on (Mg,Fe)O

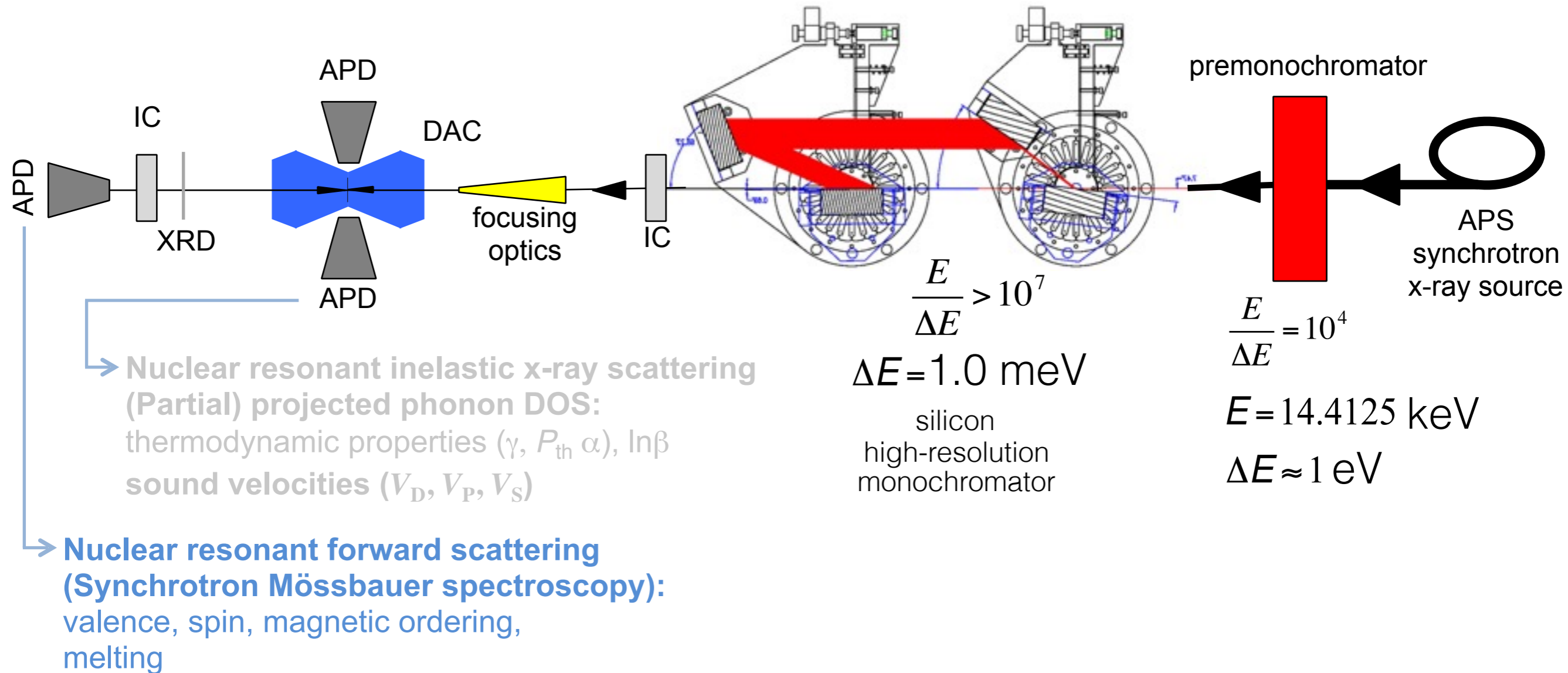
| FeO % | Methods | Pressure Mediums | Pressure Scales | Spin Transition Pressure |
|--|---|--|--|---|
| MgO  FeO | <ul style="list-style-type: none"> ○ Conventional Mössbauer ○ X-ray emission ○ Powdered x-ray diffraction ○ Single-crystal x-ray diffraction ○ Synchrotron Mössbauer ○ Optical absorption | <ul style="list-style-type: none"> ○ None ○ Boron epoxy ○ NaCl ○ KCl ○ Ar ○ Alcohol mixtures ○ Ne ○ He | <ul style="list-style-type: none"> ○ Ruby ○ NaCl ○ Pt ○ Au | <ul style="list-style-type: none"> ○ 50% volume collapse ○ 50% low spin population ○ Spin pairing energy = crystal field splitting energy ○ Visual inspection of data |

Fit a spin crossover equation of state to previous pressure-volume data sets for compositions ranging from 10-60 mol% FeO.

Compare resulting equation of state parameters.

Directly compare to results from Mössbauer spectroscopy, which is sensitive to iron's spin state.

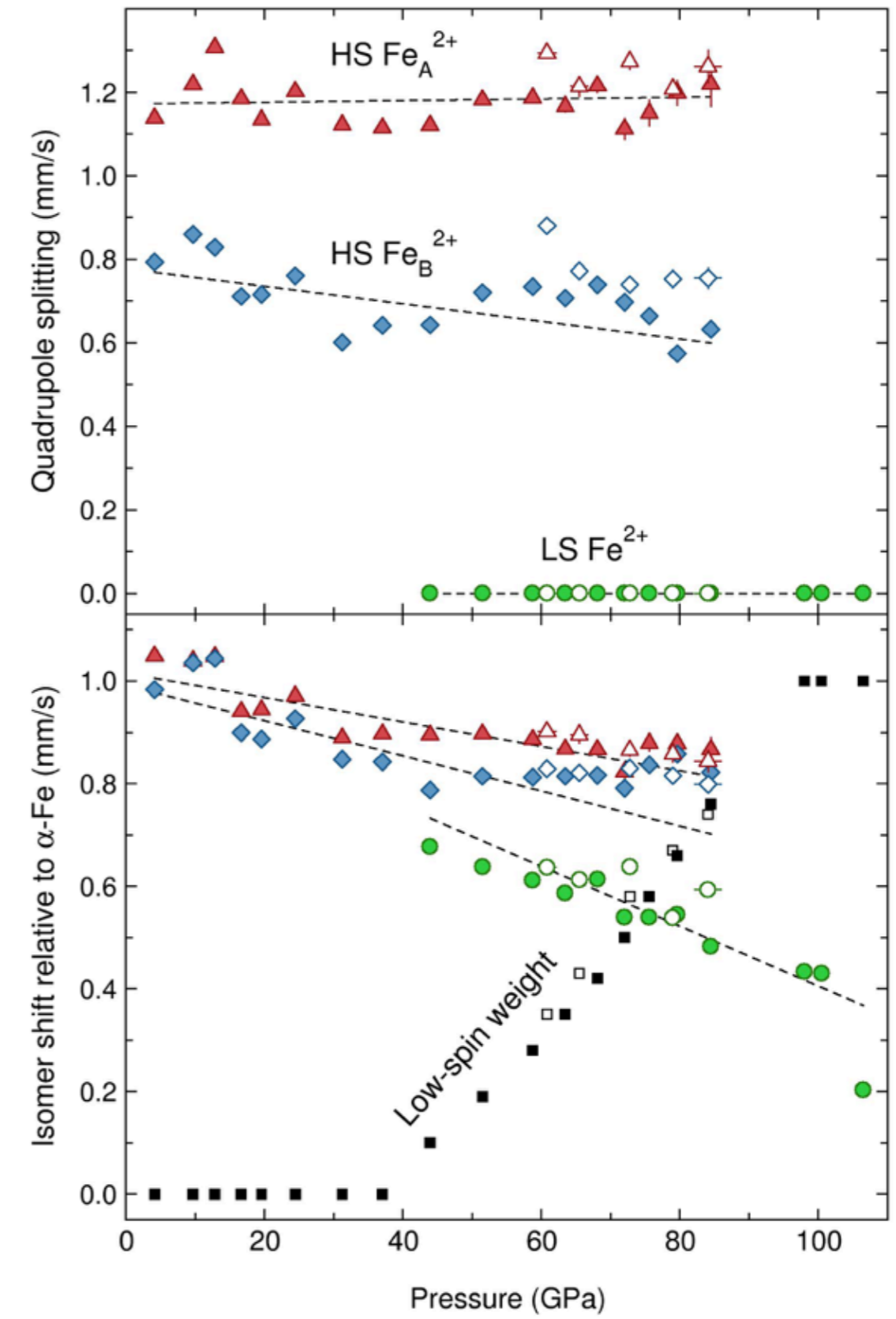
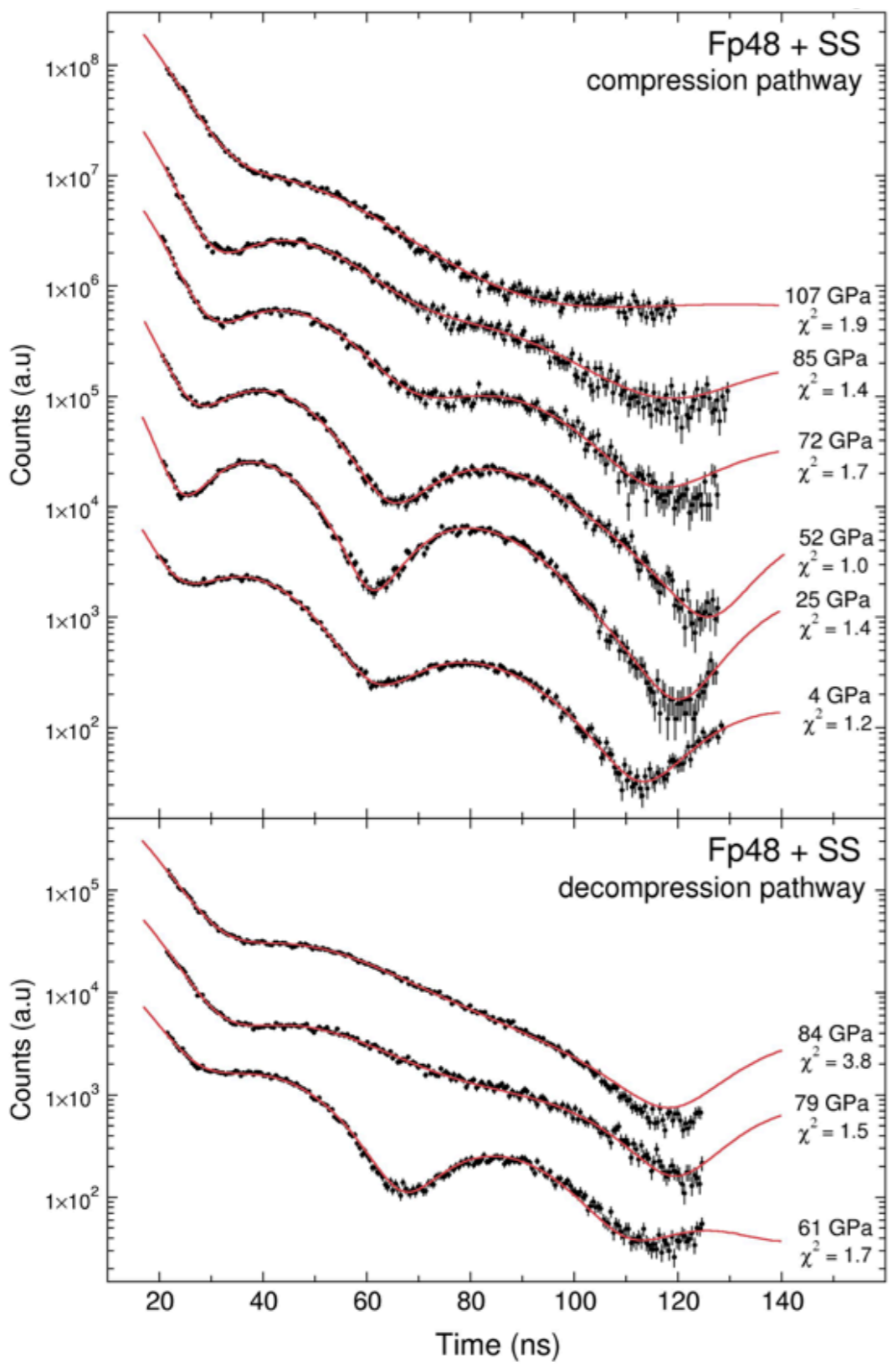
Experimental setup for nuclear resonant scattering: Sector 3-ID-B, Advanced Photon Source



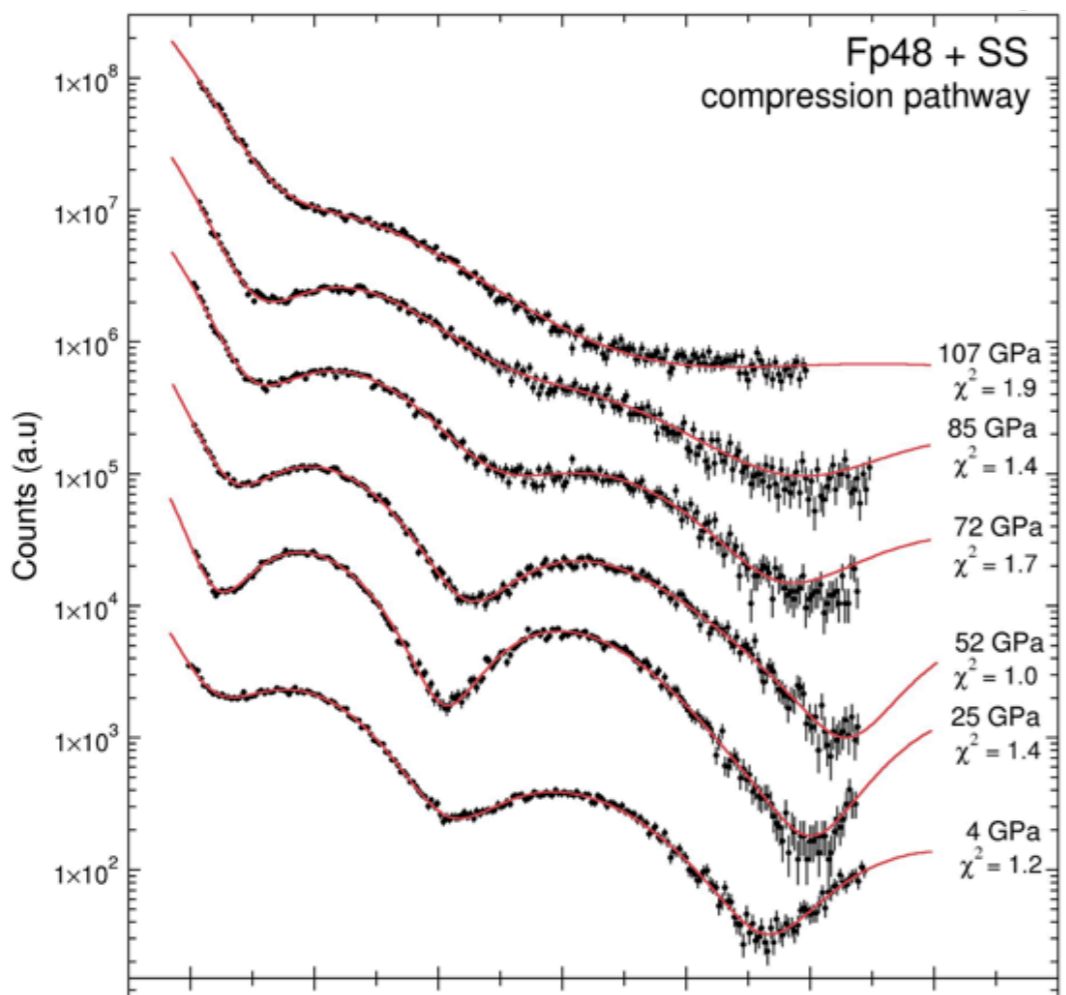
e.g., Sturhahn (*JCPM* 2004); Toellner (*HI* 2000, *JSR* 2011);
 Sturhahn & Jackson (*GSA* 2007); Jackson (*Springer* 2010)



Synchrotron Mössbauer spectroscopy study of (Mg,Fe)O

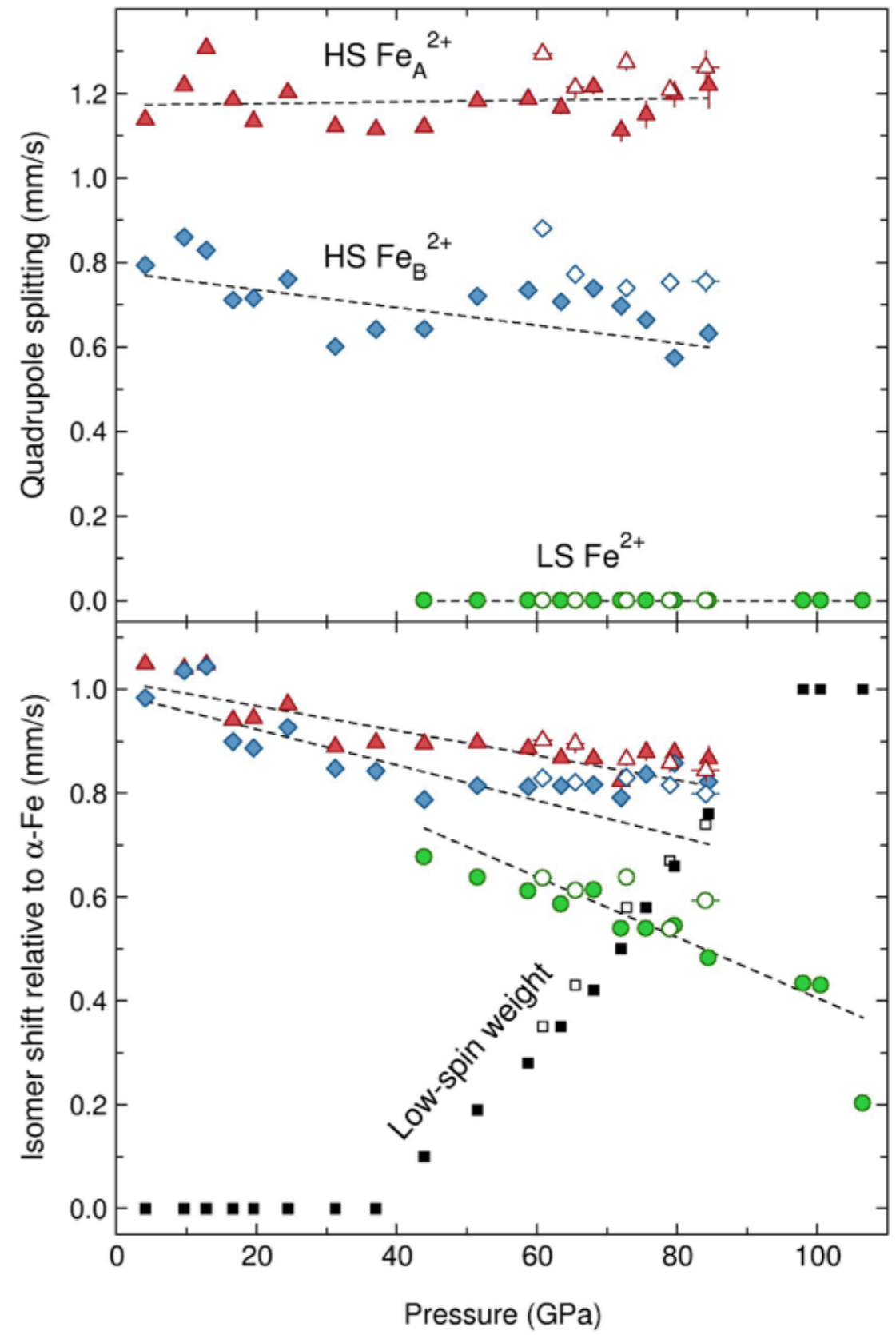
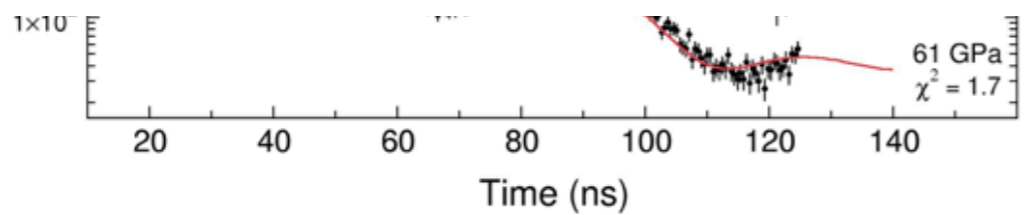


Synchrotron Mössbauer spectroscopy study of (Mg,Fe)O

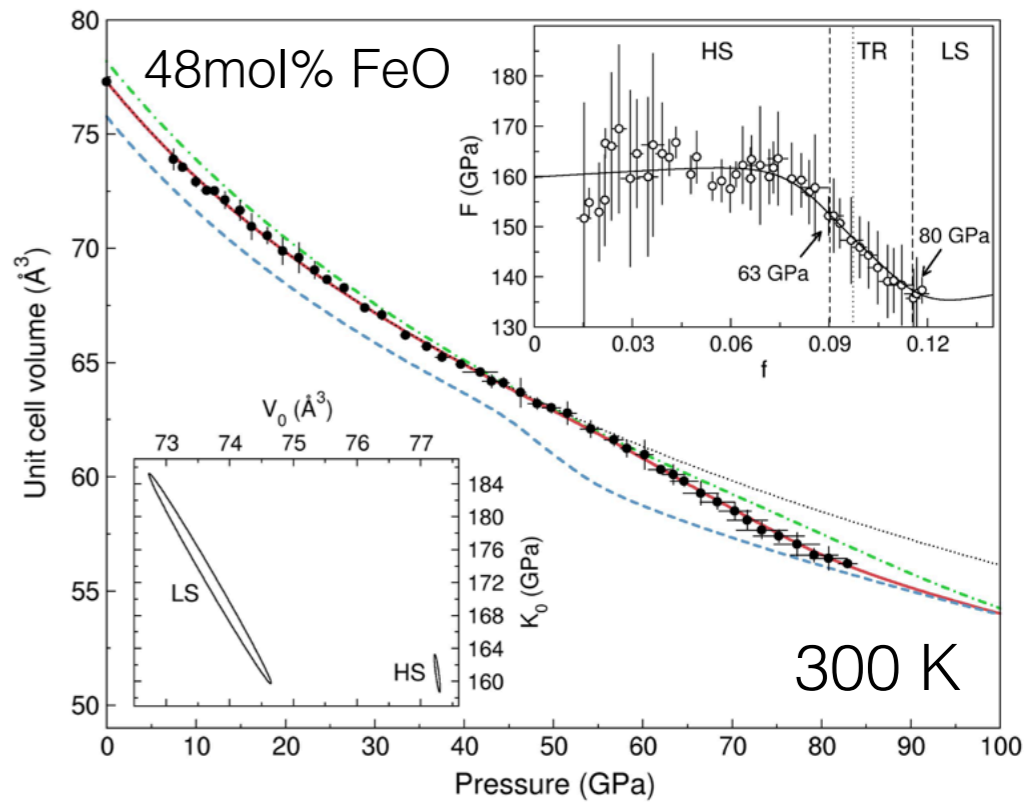
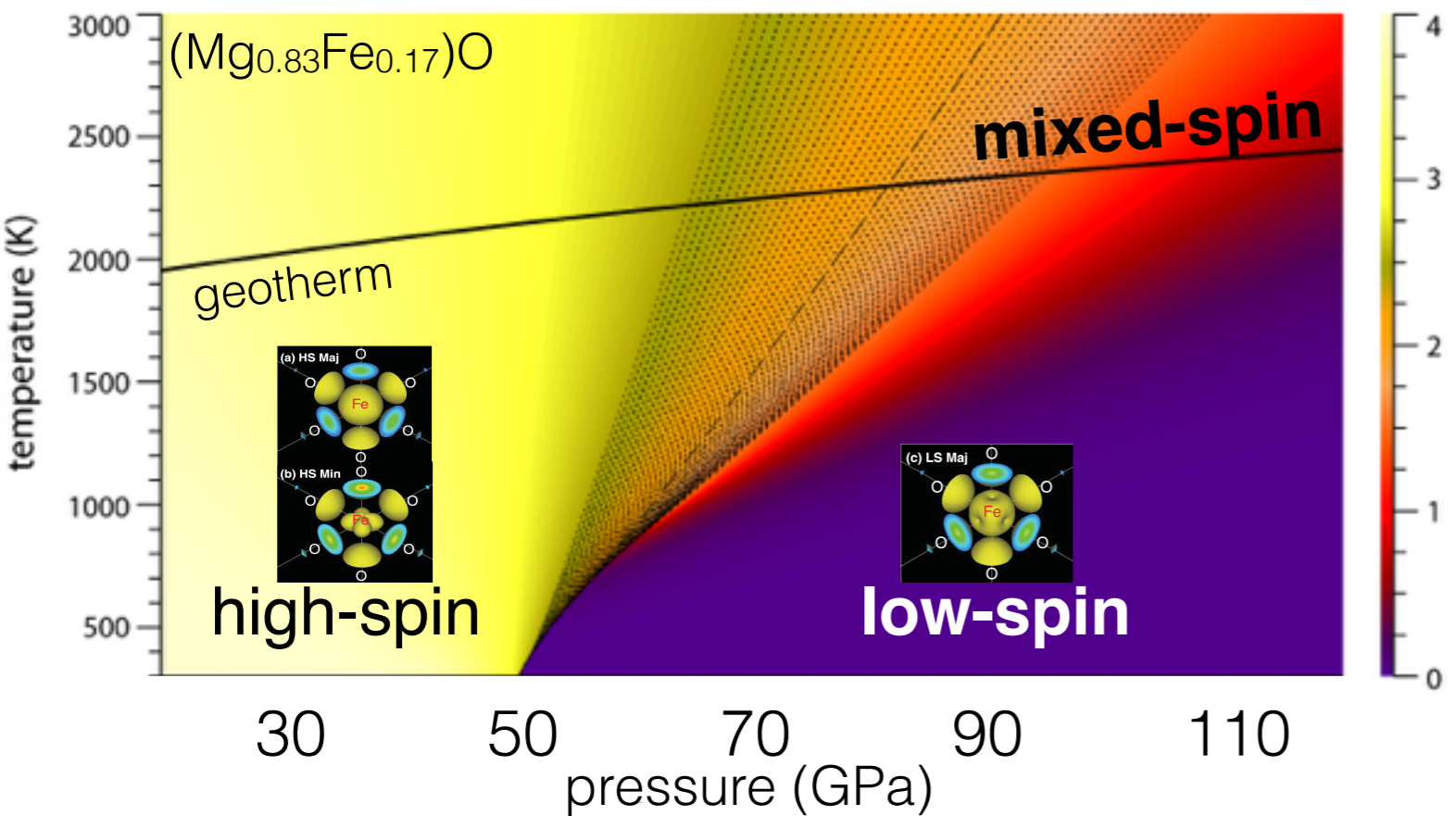


| | Fe _A ²⁺ QS | Fe _B ²⁺ QS | Fe _A ²⁺ IS | Fe _B ²⁺ IS | Fe _{L5} ²⁺ IS |
|-----------------------------------|----------------------------------|----------------------------------|----------------------------------|----------------------------------|-----------------------------------|
| Fe _A ²⁺ QS | 1.000 | -0.144 | -0.756 | 0.024 | 0.433 |
| Fe _B ²⁺ QS | -0.144 | 1.000 | 0.276 | -0.693 | 0.543 |
| Fe _A ²⁺ IS | -0.756 | 0.276 | 1.000 | -0.146 | -0.094 |
| Fe _B ²⁺ IS | 0.024 | -0.693 | -0.146 | 1.000 | -0.503 |
| Fe _{L5} ²⁺ IS | 0.433 | 0.543 | -0.094 | -0.503 | 1.000 |

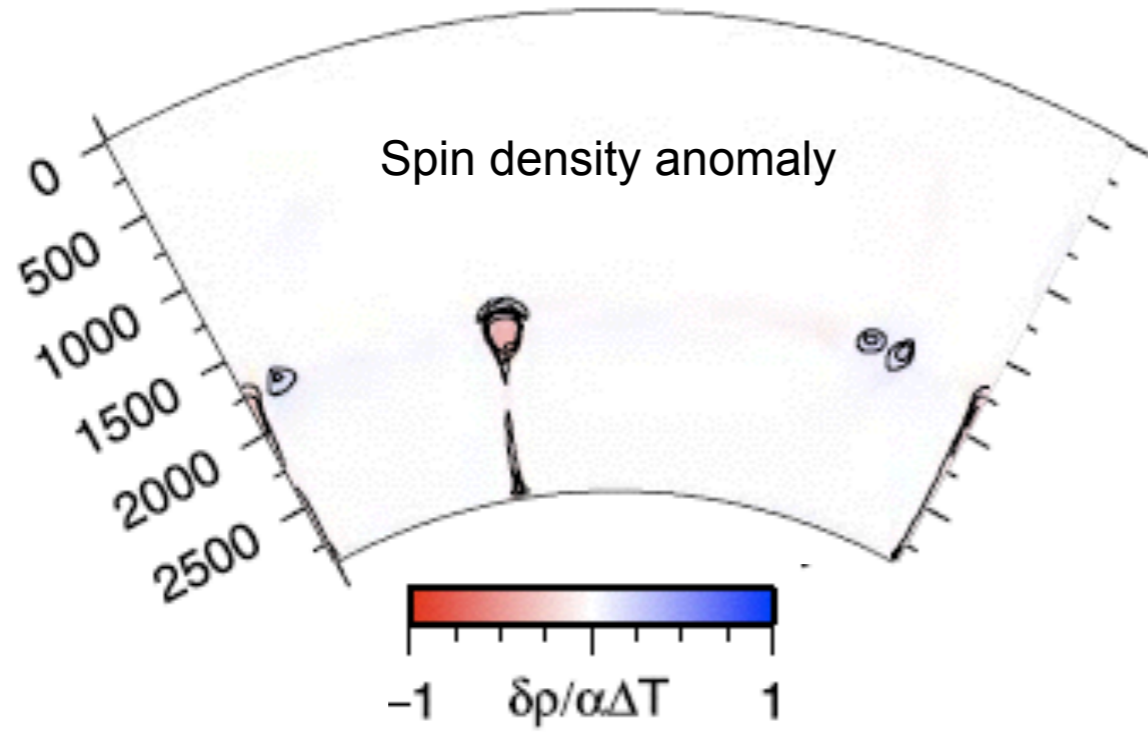
Notes: Thickness, thickness distribution, the QS distribution, and weight fractions of the different sites were fixed. The QS of Fe_{L5}²⁺ was fixed to 0.



Ferropericlase spin buoyancy



Solomatova et al. Am. Min. (2016)



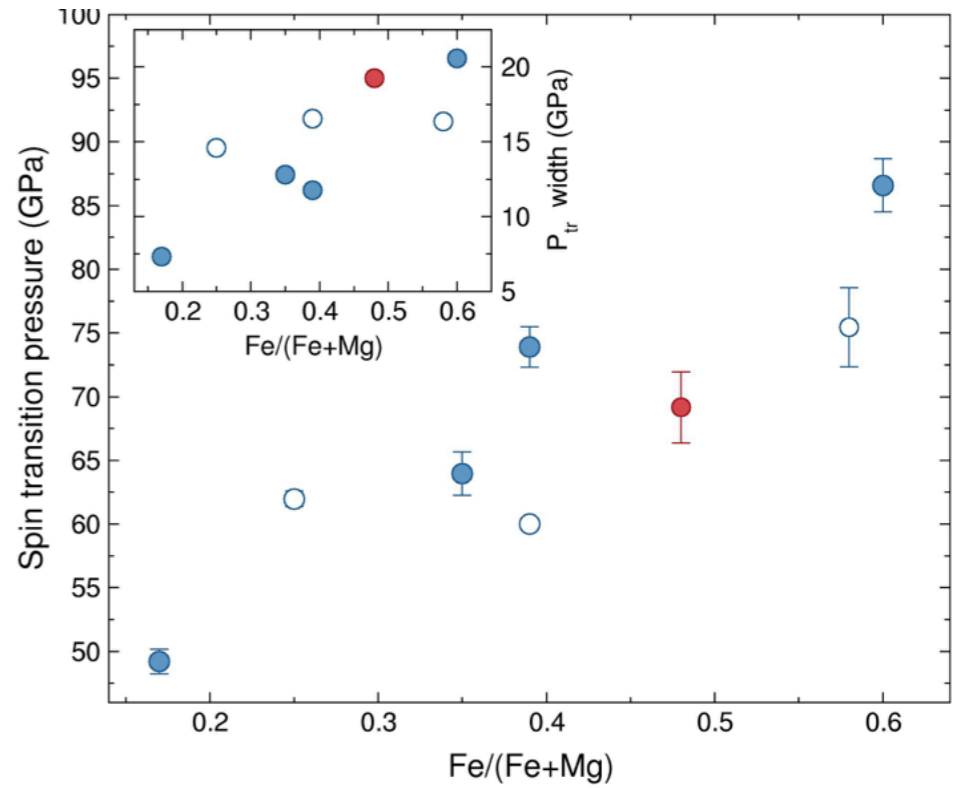
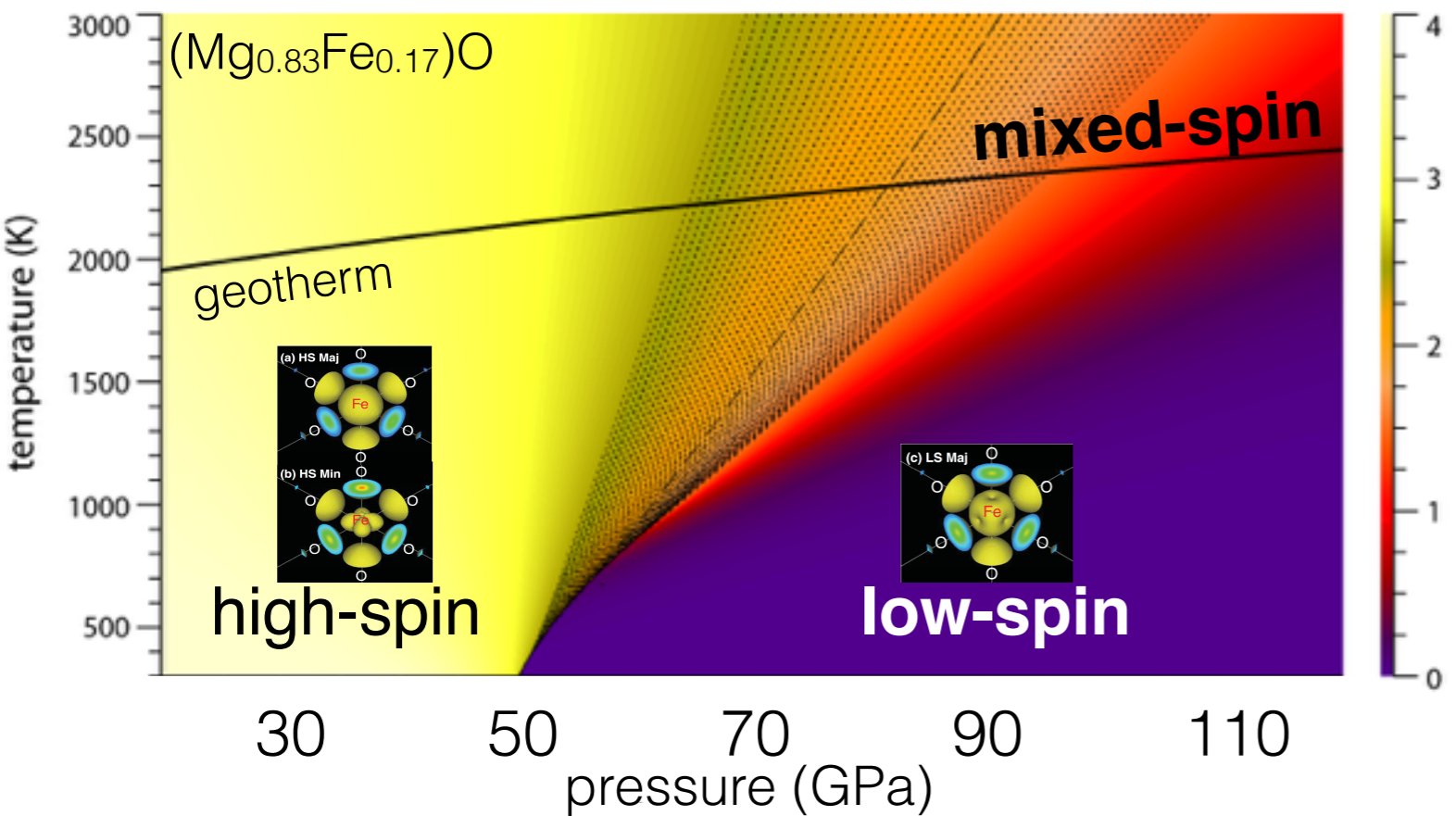
Compare with first principles at 300 K:
Tsuchiya et al. (2006):

$P_{spinTr} = 36 \text{ GPa}$
 $Width_{spinTr} = 4 \text{ GPa}$

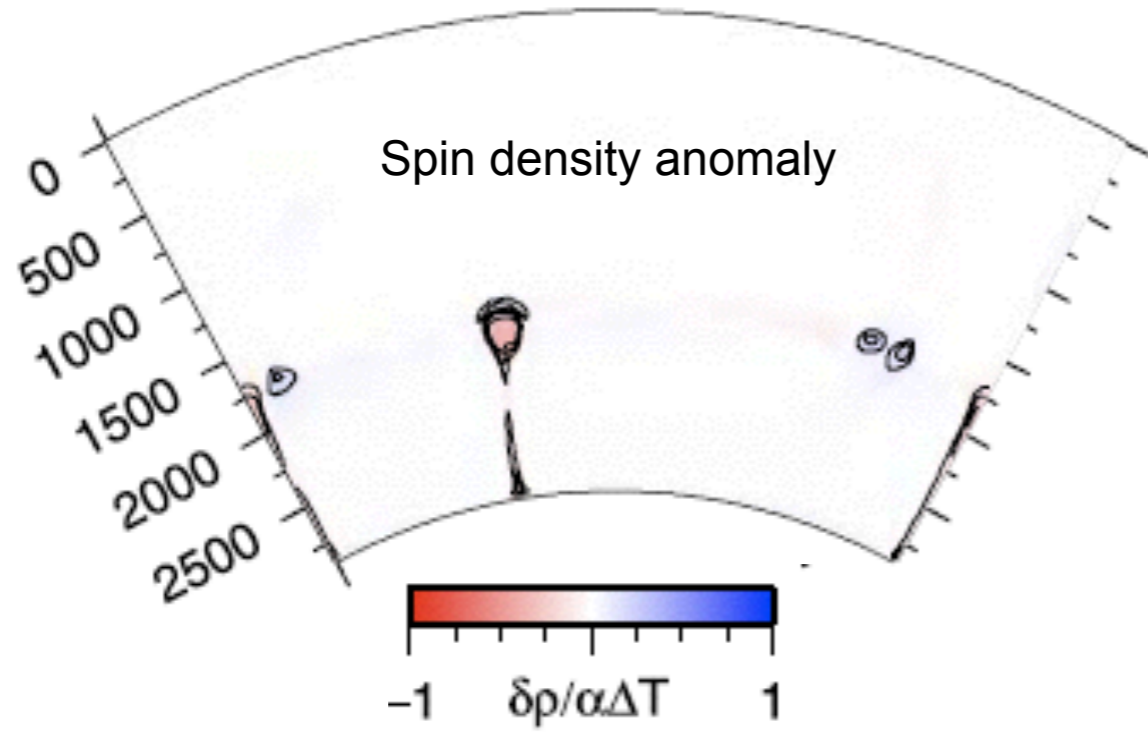
Holström & Stixrude (2015):

$P_{spinTr} = 65 \text{ GPa}$
 $Width_{spinTr} = 50 \text{ GPa}$

Ferropericlase spin buoyancy



Solomatova et al. Am. Min. (2016)



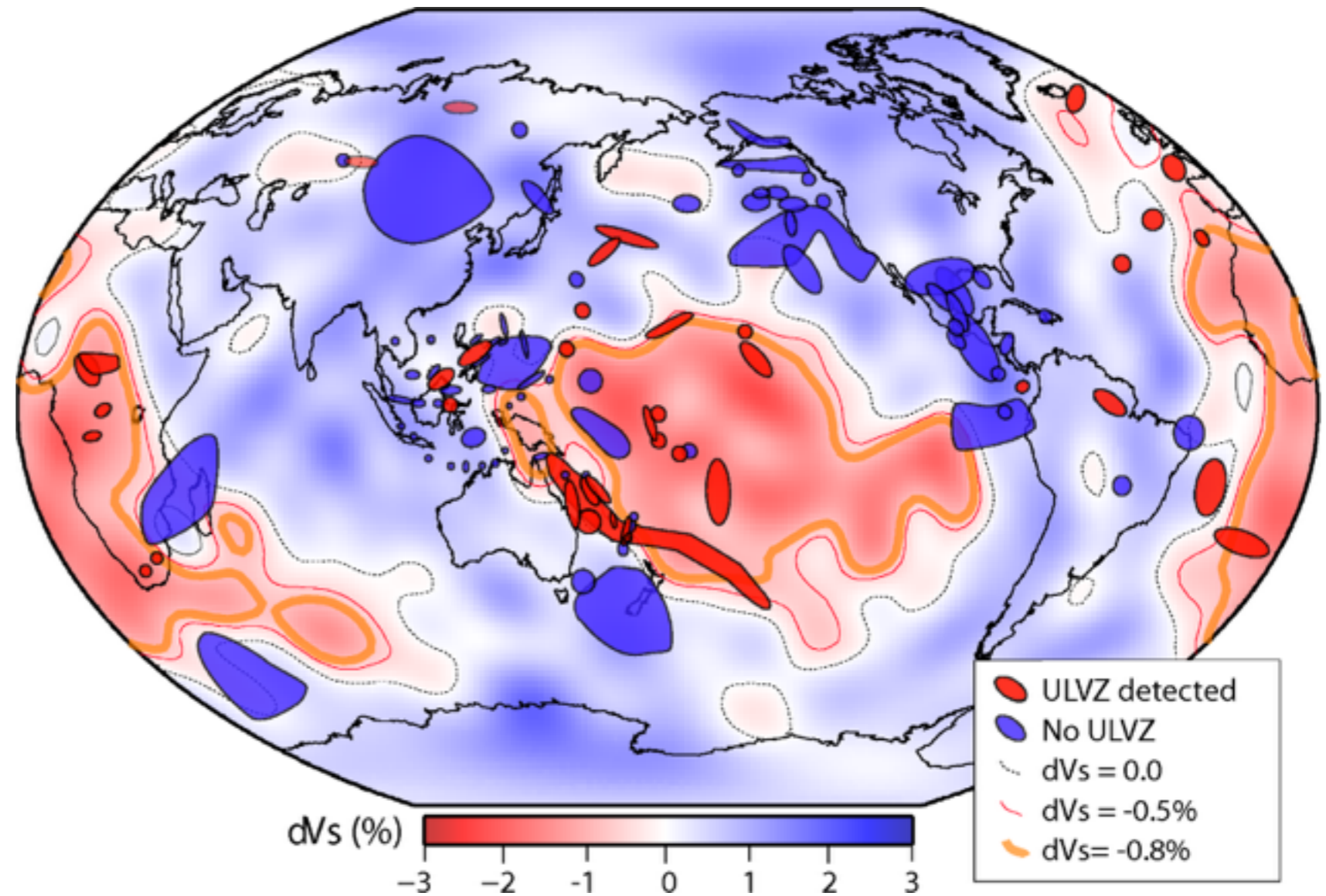
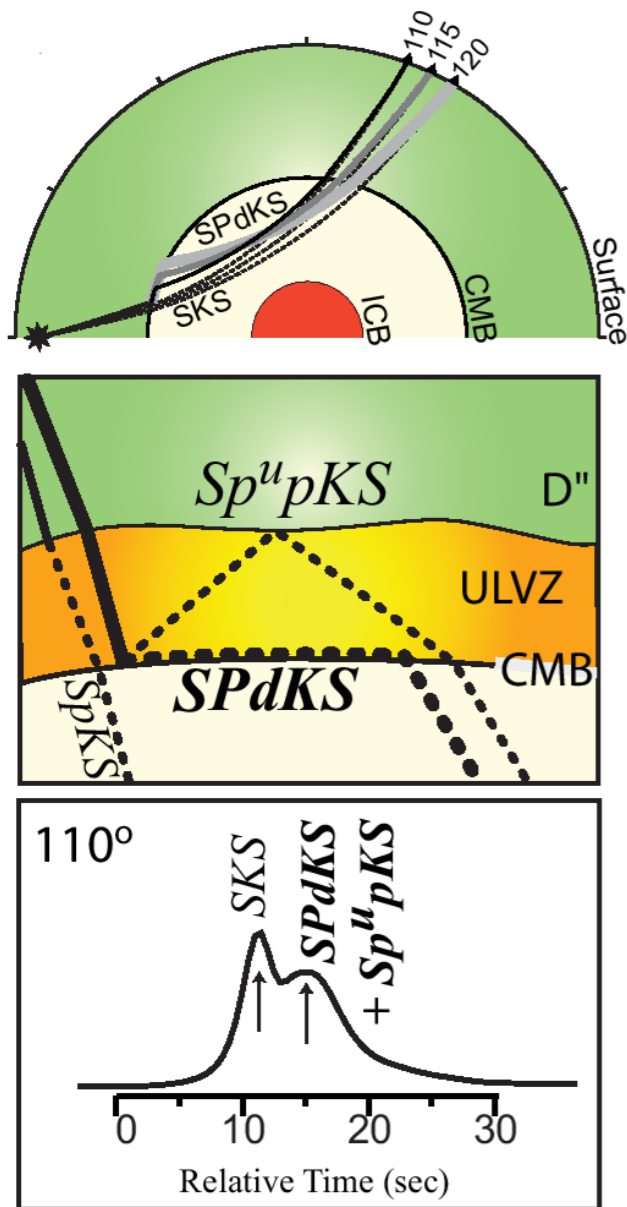
Compare with first principles at 300 K:
Tsuchiya et al. (2006):

$P_{spinTr} = 36 \text{ GPa}$
 $Width_{spinTr} = 4 \text{ GPa}$

Holström & Stixrude (2015):

$P_{spinTr} = 65 \text{ GPa}$
 $Width_{spinTr} = 50 \text{ GPa}$

Distribution of low velocity zones at the base of the mantle



Slow

5 to 20% drop in V_P
10 to 30% drop in V_S

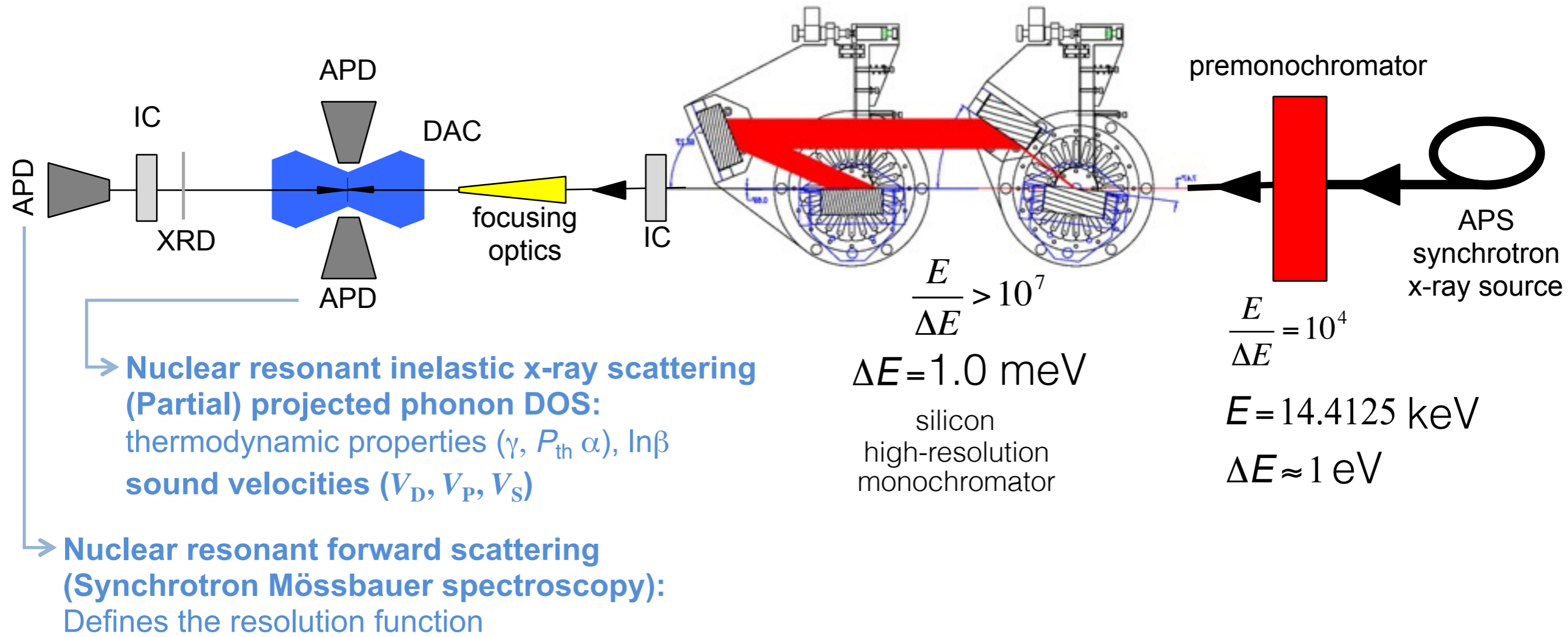
V_P/V_S

Variable
Not well-constrained

Dense

4 to 14% denser
Not well-constrained

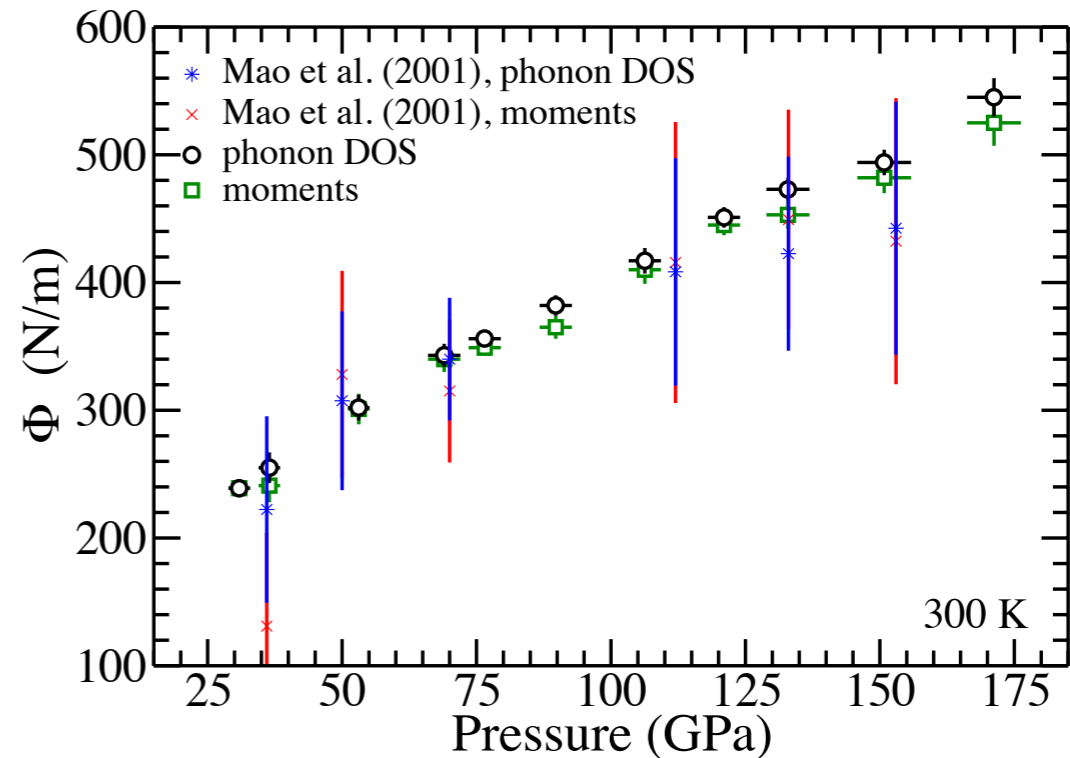
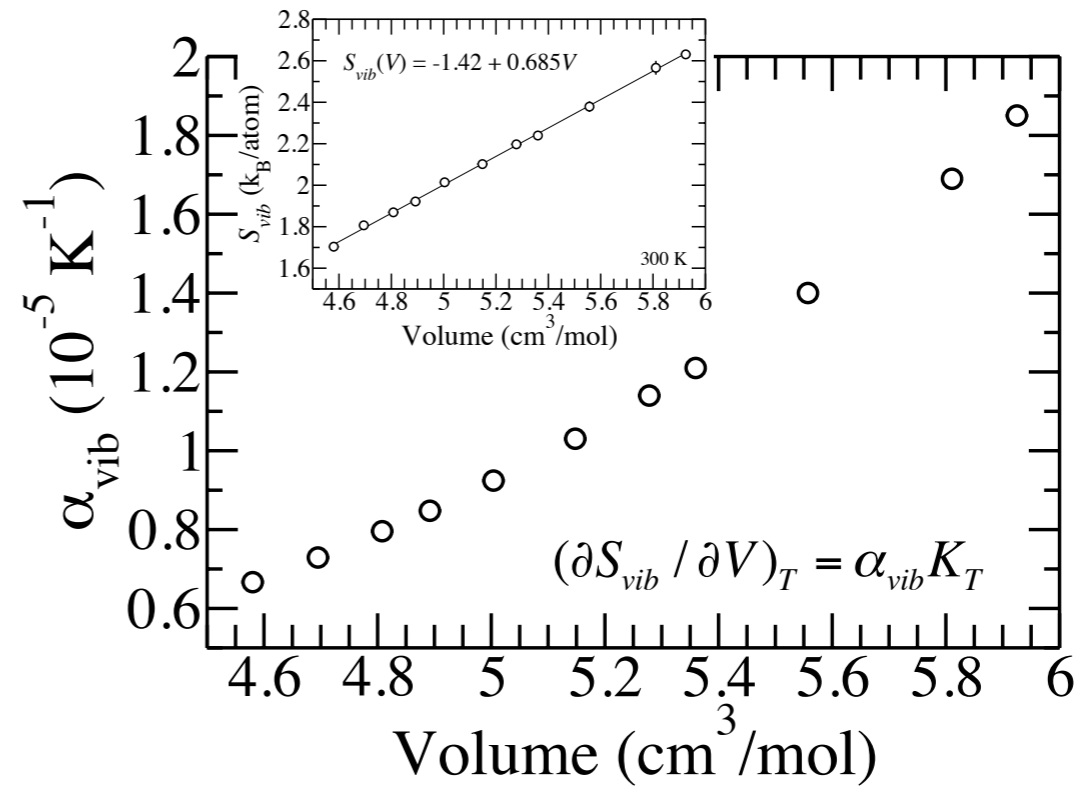
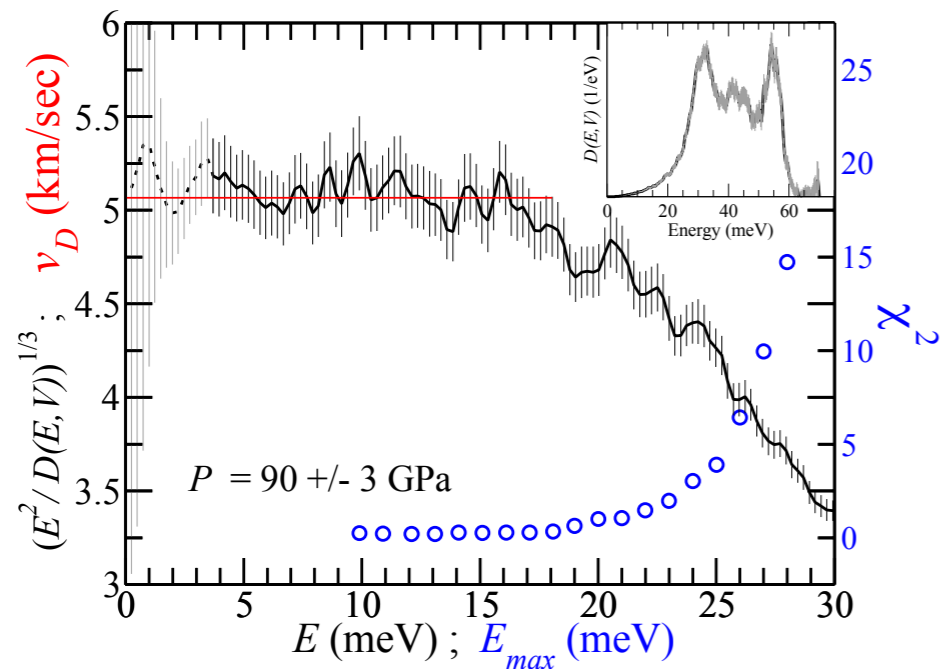
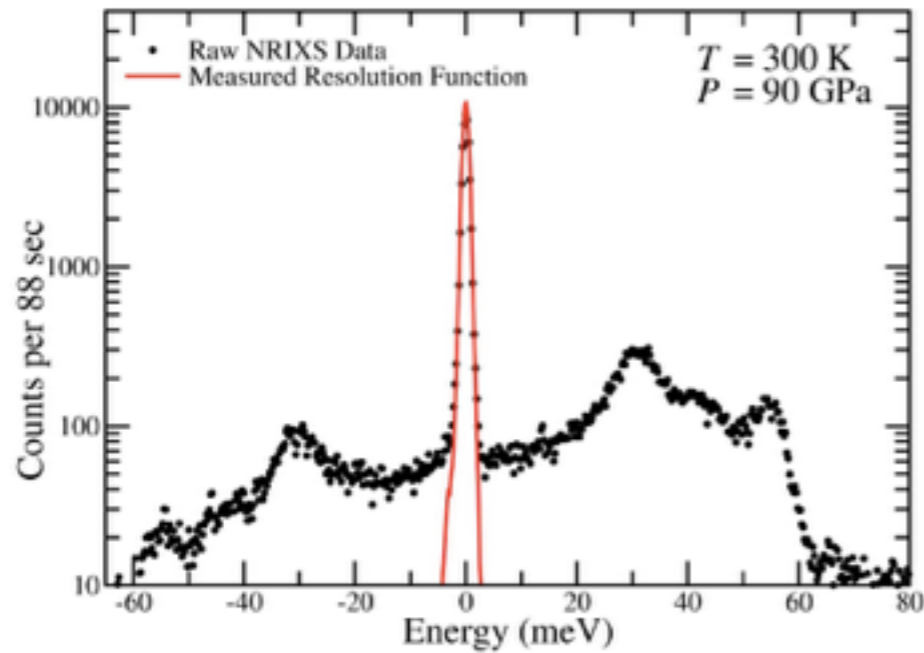
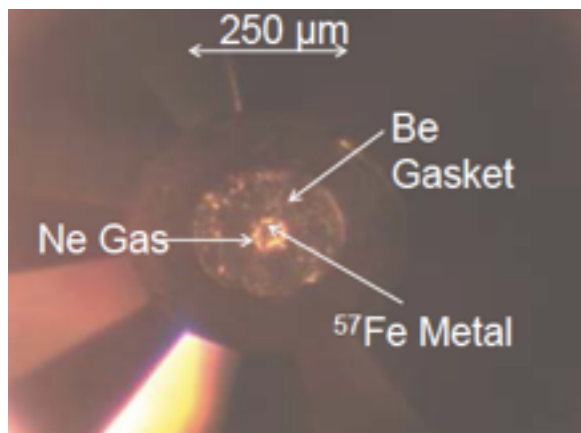
Experimental setup for nuclear resonant inelastic scattering: Sector 3-ID-B, Advanced Photon Source



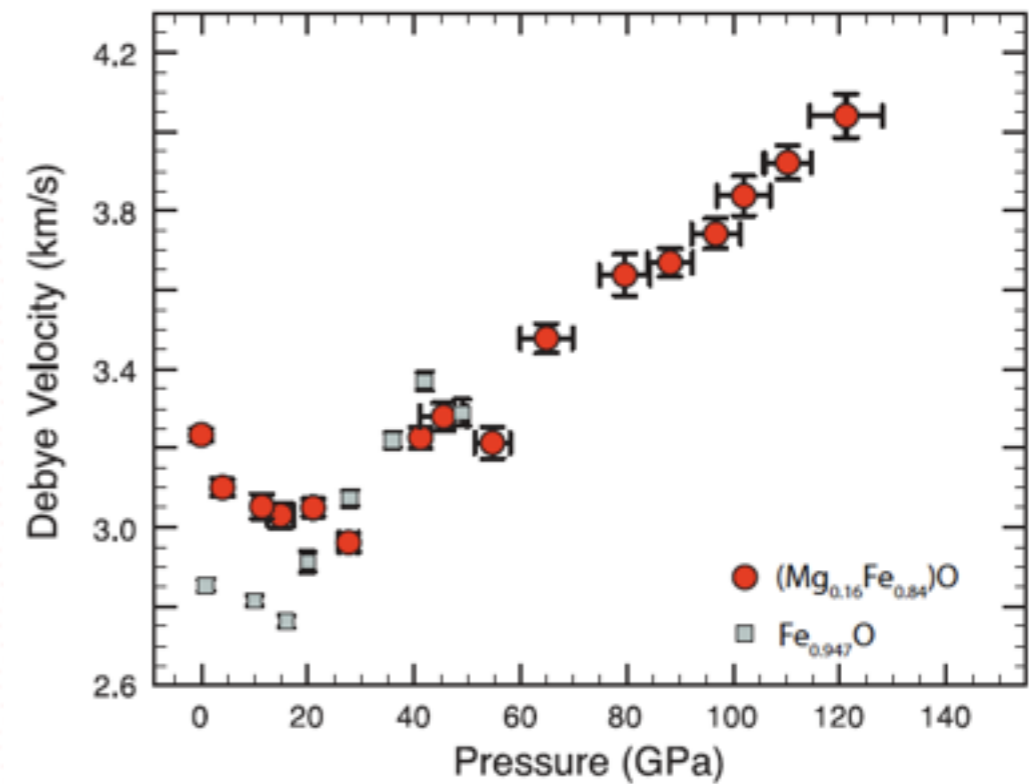
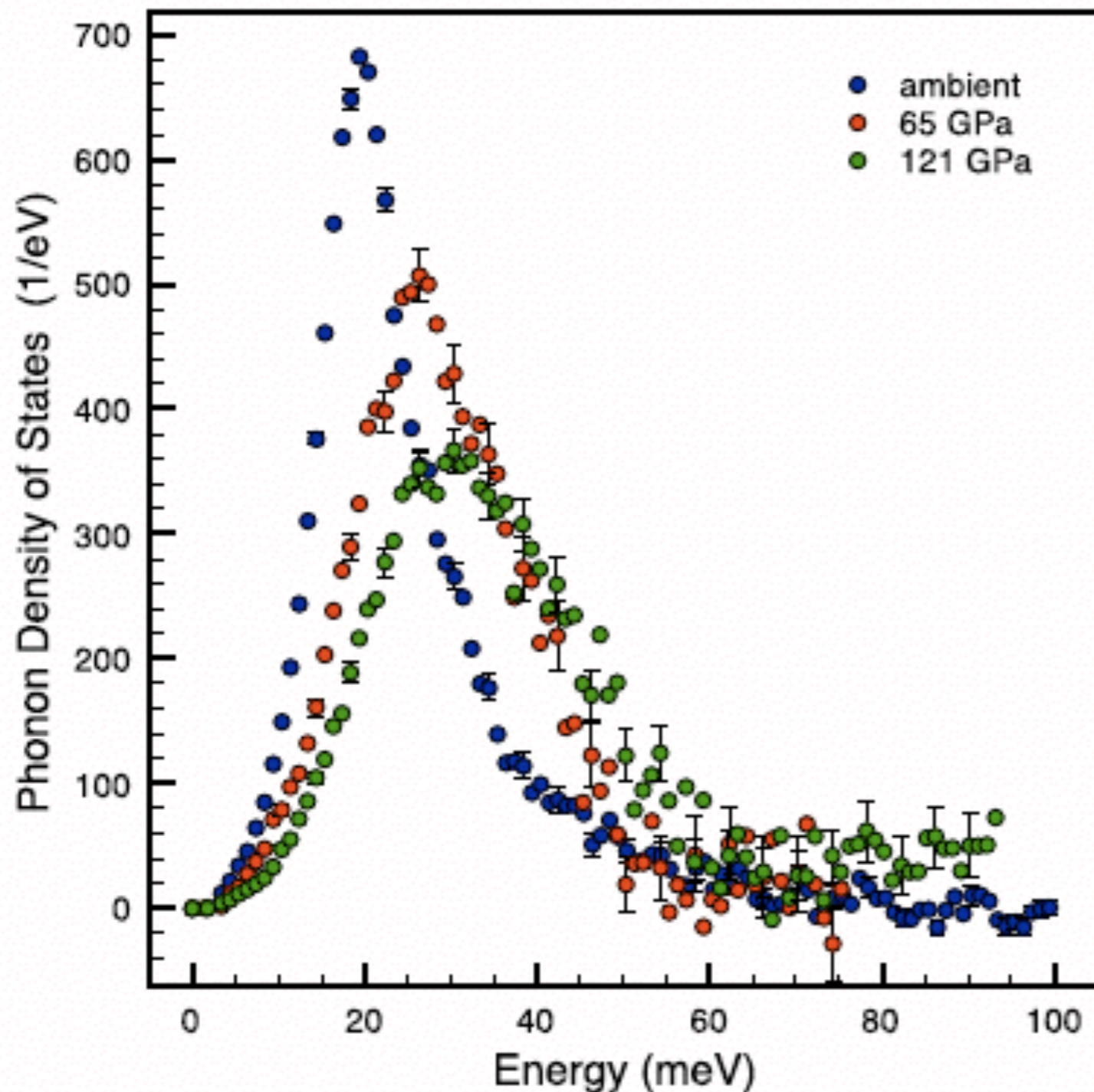
e.g., Sturhahn (*JCPM* 2004); Toellner (*HI* 2000, *JSR* 2011);
 Sturhahn & Jackson (*GSA* 2007); Jackson (*Springer* 2010)



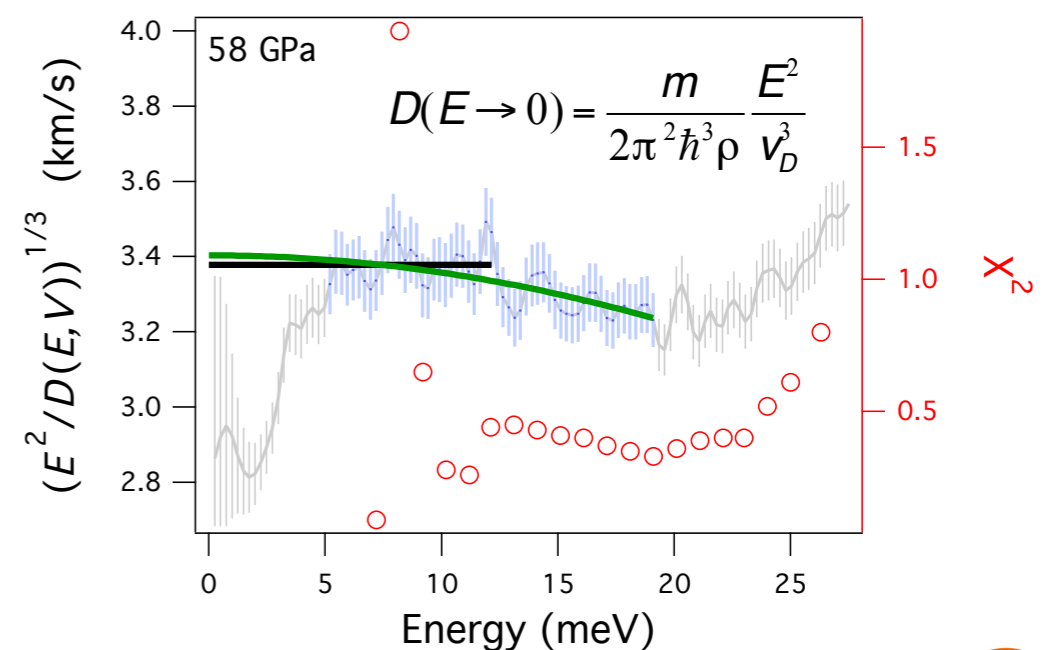
Volume dependence of the phonon DOS for *hcp*-iron to outer core pressures



Partial phonon density of states of iron-rich (Mg,Fe)O magnesiowüstites

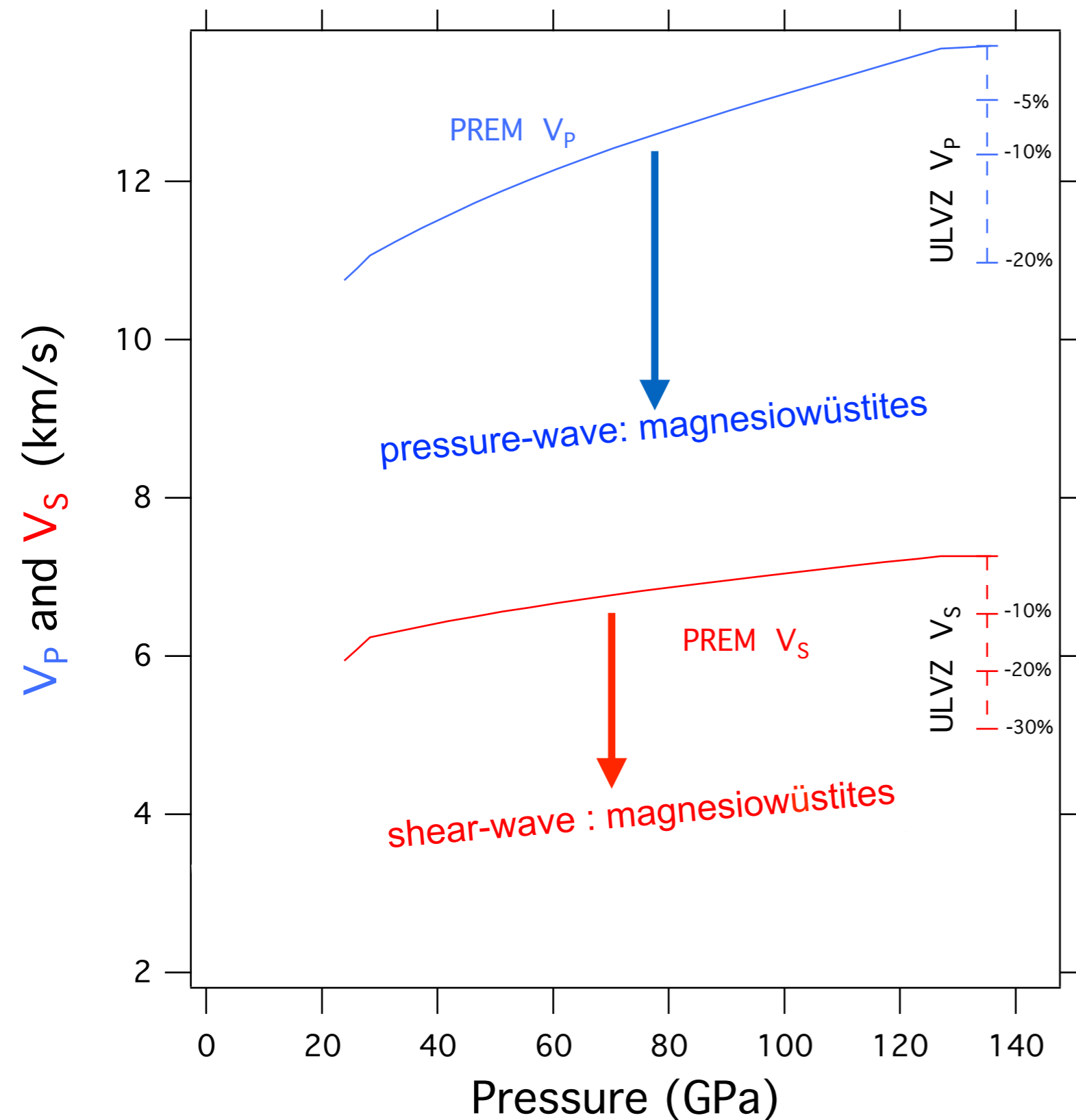


(Mg_{0.06}Fe_{0.94})O: Debye velocity, V_D

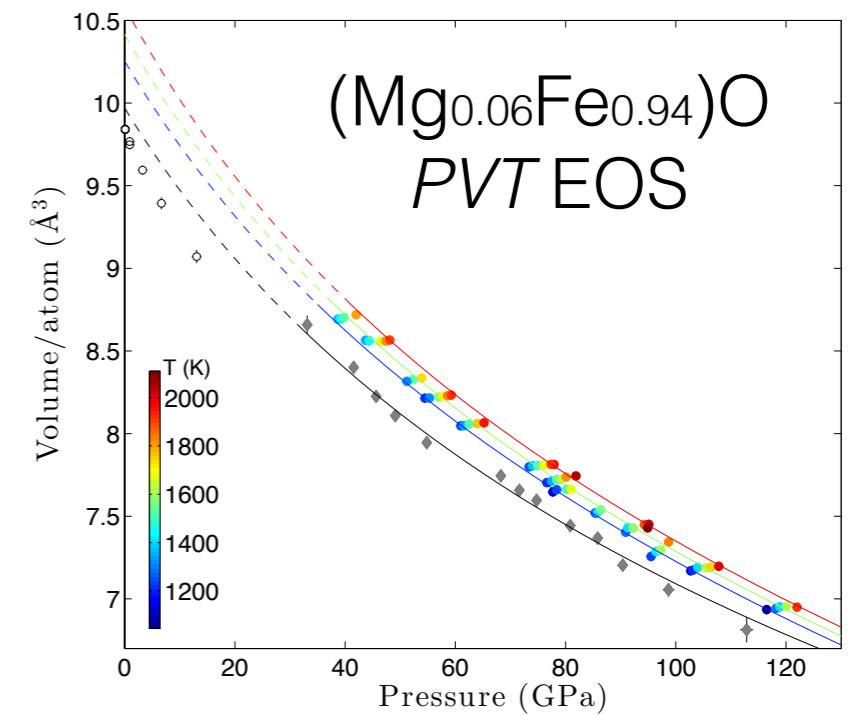


Ultralow-velocities in magnesiowüstites

(Mg_{0.16}Fe_{0.84})O, (Mg_{0.06}Fe_{0.94})O, FeO



V_P and V_S

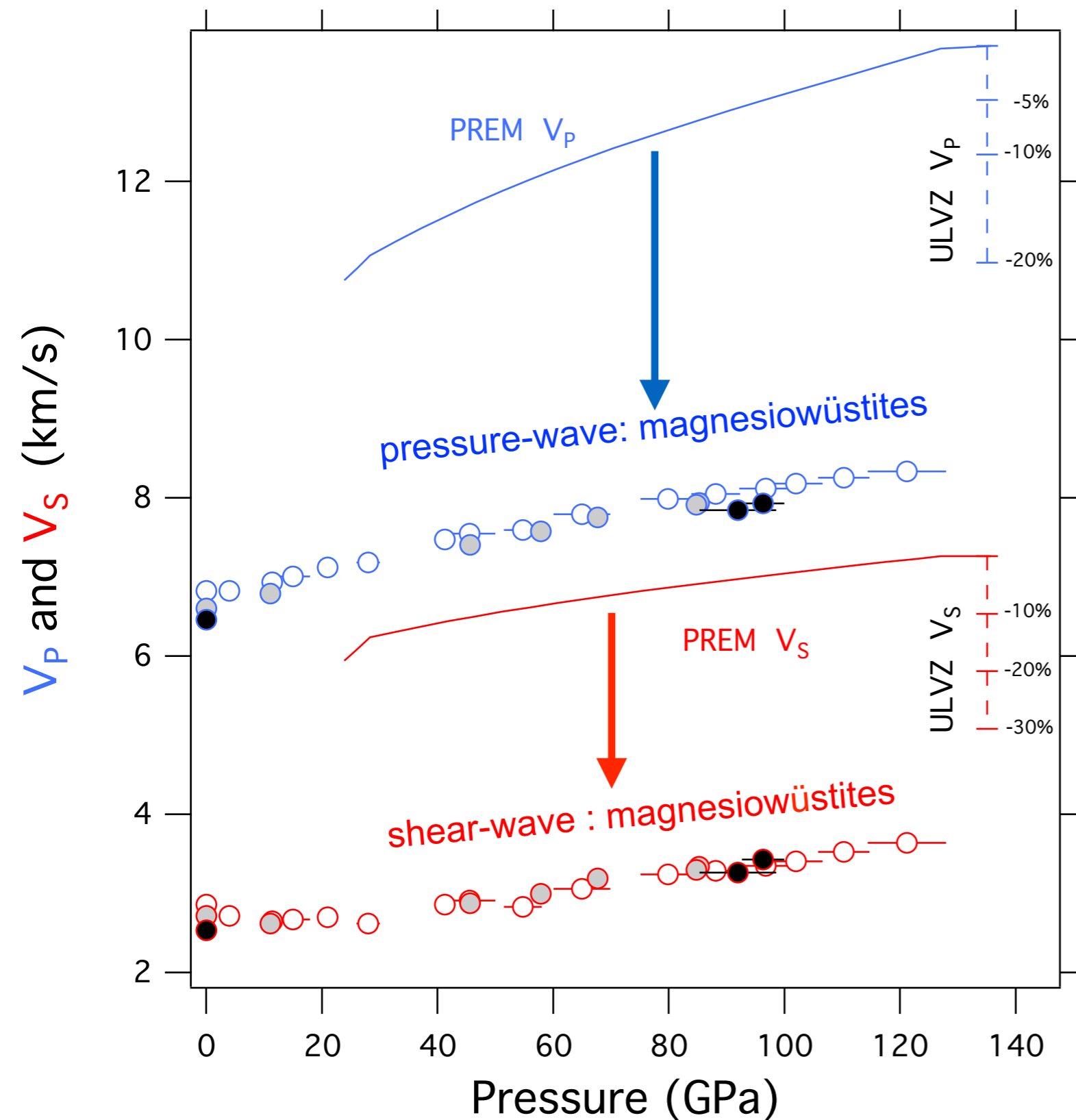


$$\frac{3}{V_D^3} = \frac{1}{V_P^3} + \frac{2}{V_S^3}$$

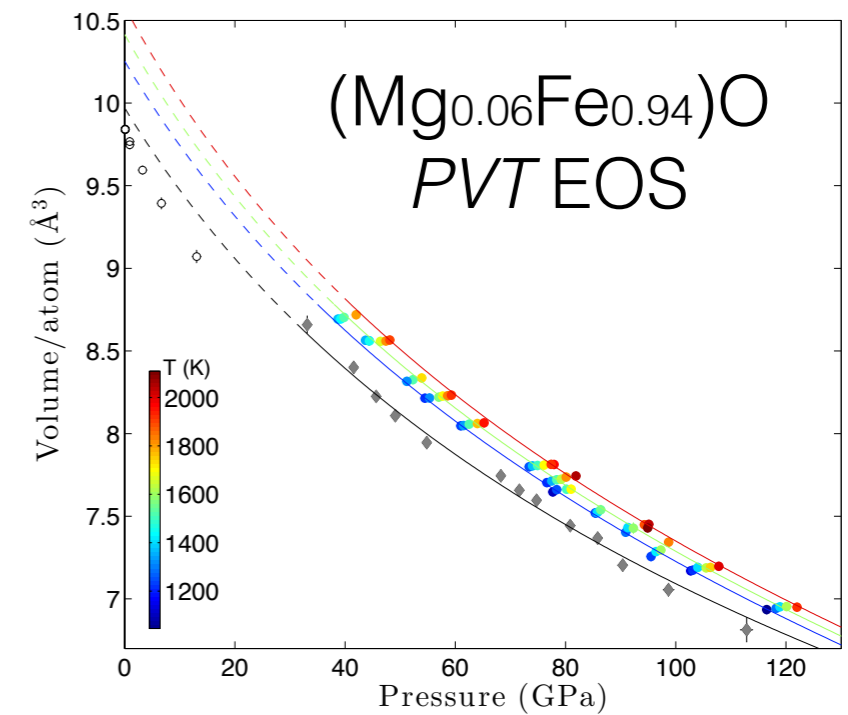
$$\frac{K_S}{\rho} = V_P^2 - \frac{4}{3} V_S^2$$

Ultralow-velocities in magnesiowüstites

(Mg_{0.16}Fe_{0.84})O, (Mg_{0.06}Fe_{0.94})O, FeO



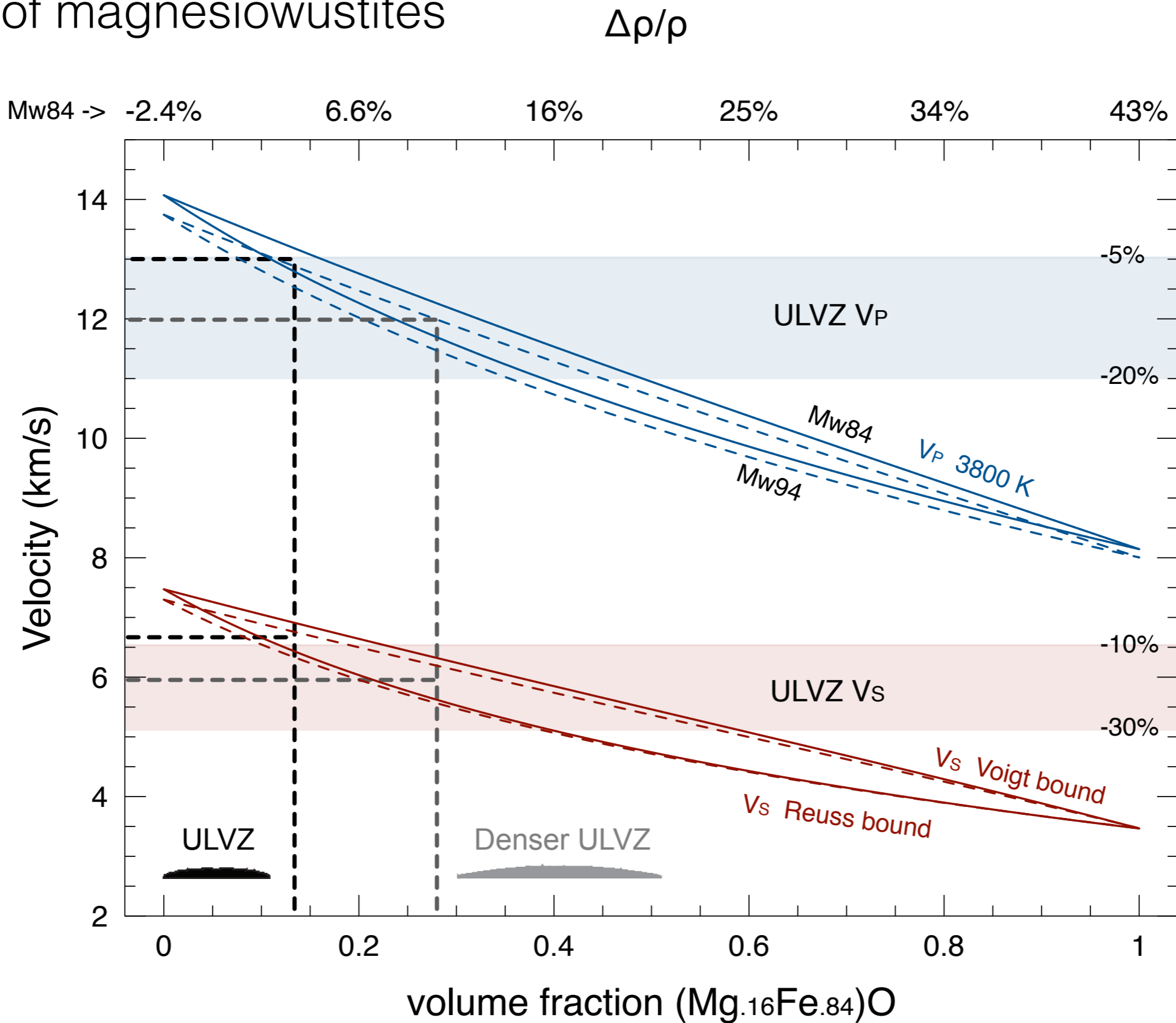
V_P and V_S



$$\frac{3}{V_D^3} = \frac{1}{V_P^3} + \frac{2}{V_S^3}$$

$$\frac{K_S}{\rho} = V_P^2 - \frac{4}{3} V_S^2$$

Self consistent model for ultralow-velocity zones: Presence of magnesiowüstites



K_D: Tange et al. JGR (2009), *dV_{P,S}/dT*: Wentzcovitch et al. (2010)
EOS: Wicks et al. PEPI (2015), Wicks et al. (2016, under revision)



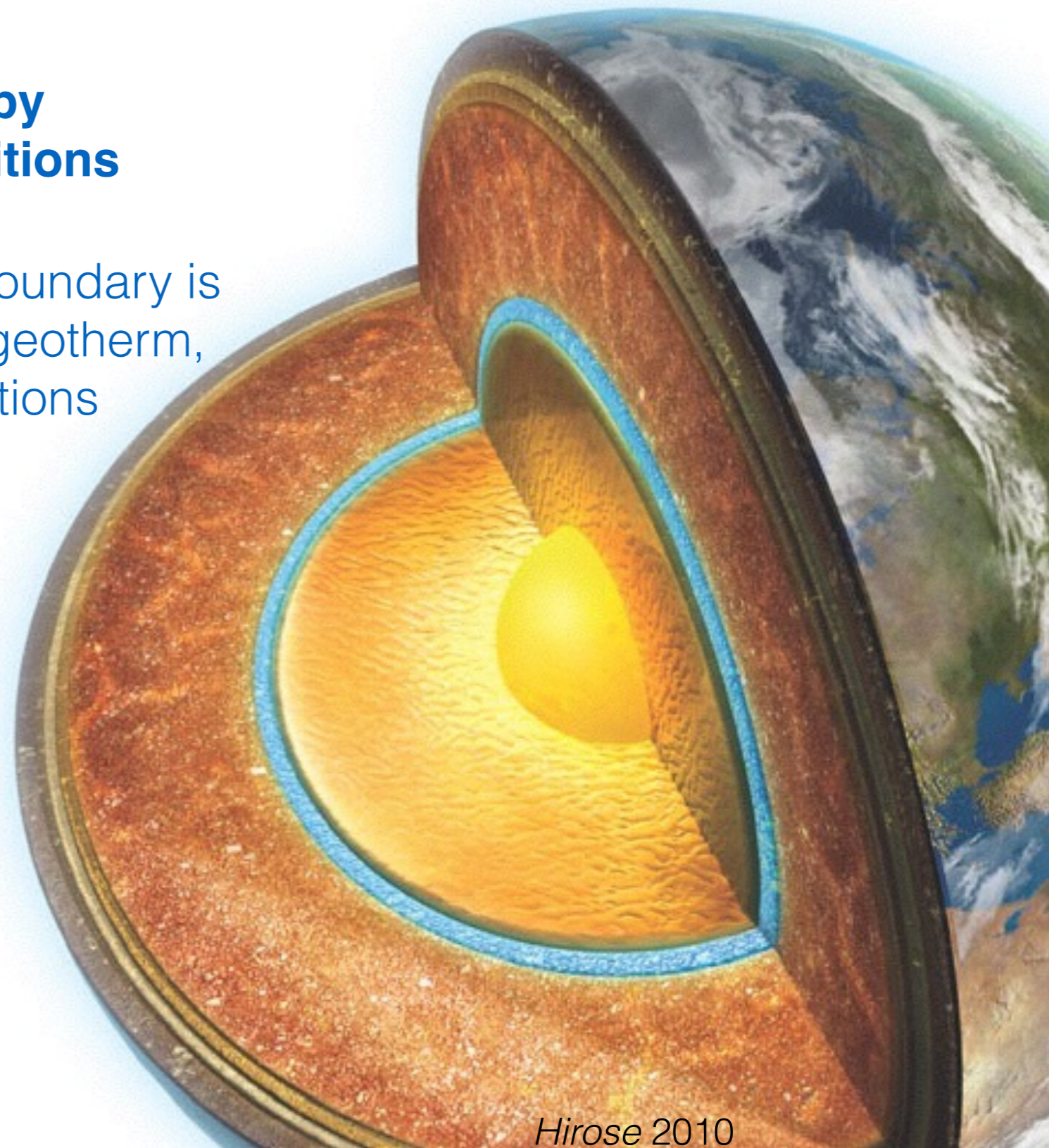
Constraining the temperature of Earth's core-mantle boundary

Phase stability dictated by pressure-temperature conditions

The temperature of the core-mantle boundary is determined from a plausible mantle geotherm, anchored by major phase transitions

**T_{CMB} remains poorly constrained:
3400 to 4400 degrees K**

Motivated to develop a technique to better constrain the thermal profile of the deep Earth



Hirose 2010

Detection of the solid – liquid boundary using synchrotron Mössbauer spectroscopy

$$f_{LM} = e^{-k^2 \langle u^2 \rangle} \Rightarrow 0$$

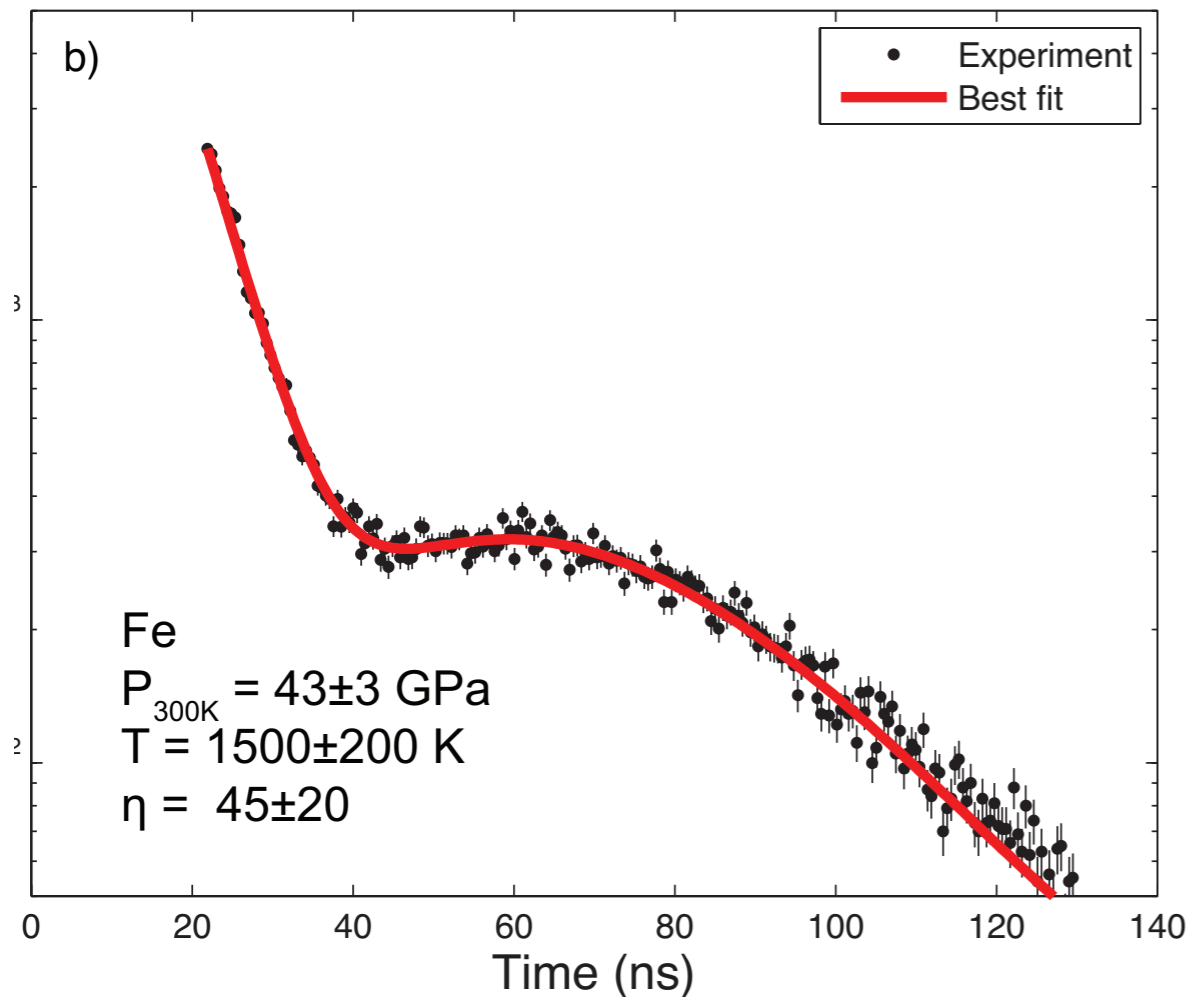
- When melting occurs: $f_{LM} = 0$
- Sensitive to the dynamics of the atoms
- Distinguishes a liquid from an amorphous state
- Near zero background
- Demonstrated for ^{119}Sn at ambient pressure using conventional Mössbauer spectroscopy
 - Boyle *et al. Proc. Phys. Soc.* 1960

Mössbauer *Z. Phys.* 1958

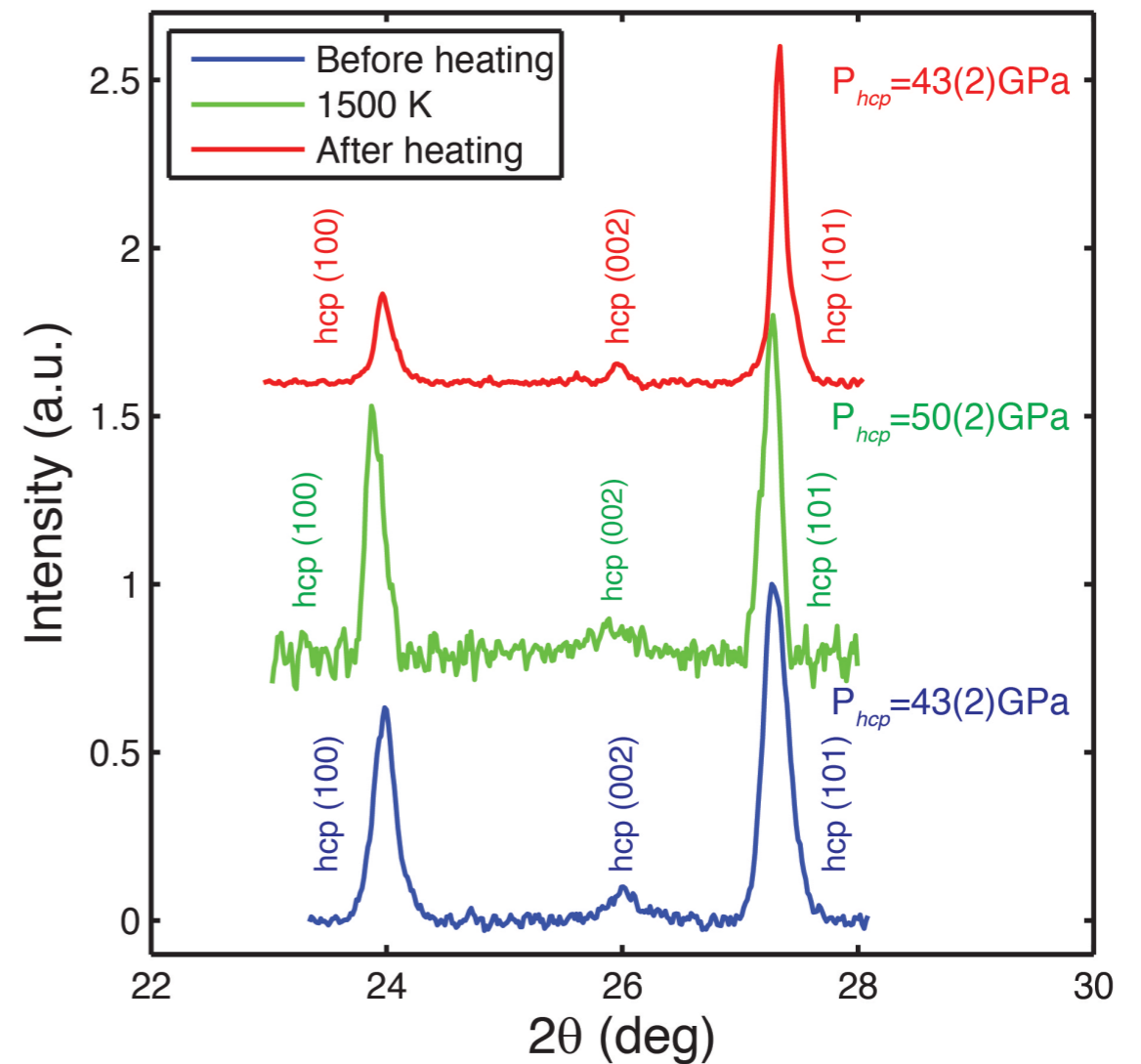
Singwi & Sjölander *Phys. Rev.* 1960

Jackson *et al. EPSL* 2013

Synchrotron Mössbauer spectroscopy: iron-alloy melting measurements



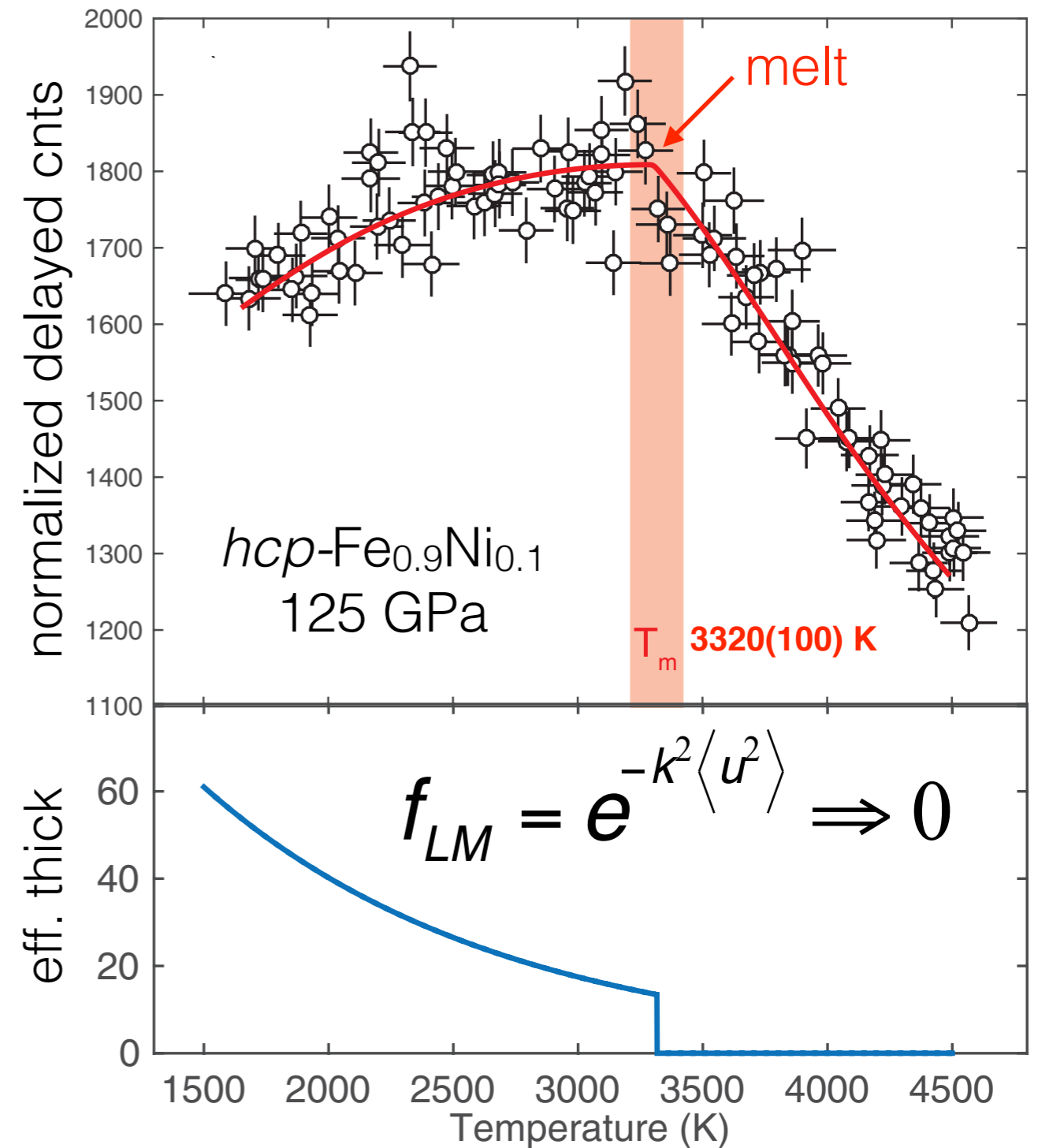
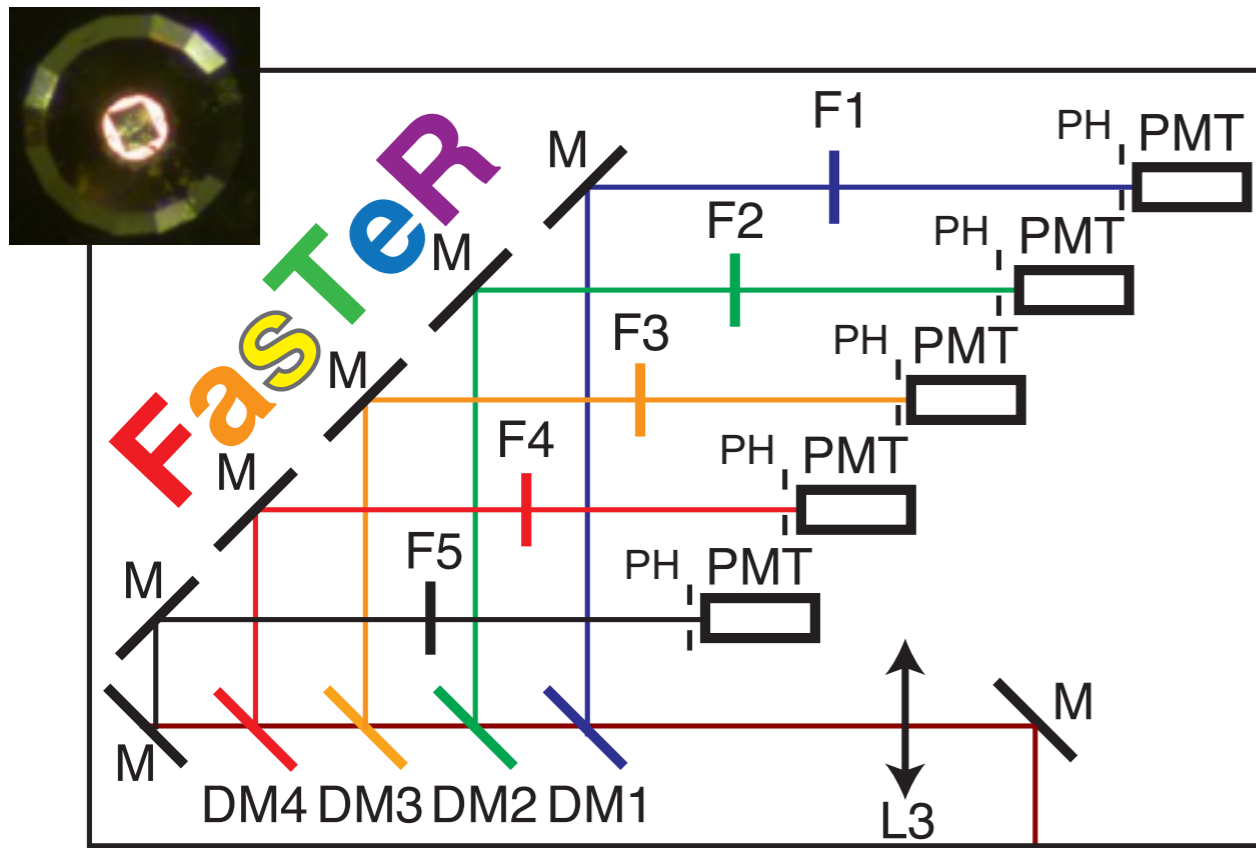
Initial effective thickness of fcc-Fe_{0.9}Ni_{0.1}
constrained from high-PT
synchrotron Mössbauer spectroscopy



Thermal pressure of sample constrained from
established equations of state and high-PT
x-ray diffraction

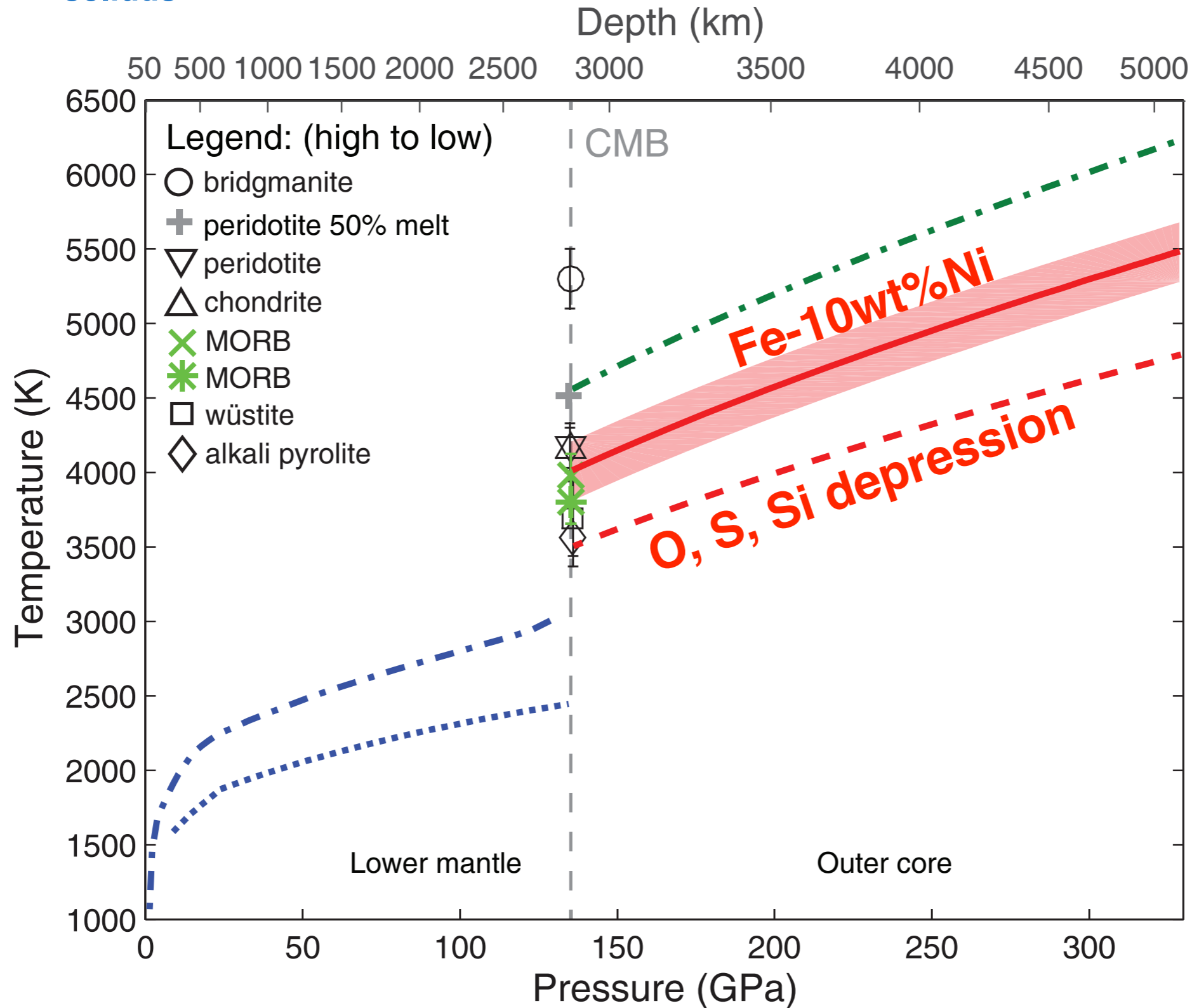
Synchrotron Mössbauer spectroscopy: melting measurements

- Signal originates only from iron-bearing sample (no background)
- Monitoring atomic dynamics at high temperatures (melting) with high precision, using XRD to constrain thermal pressure
- Fast Temperature Readout system (FasTeR): microsecond readout, up to 400 Hz
- Stokes anti-Stokes temperature calibration



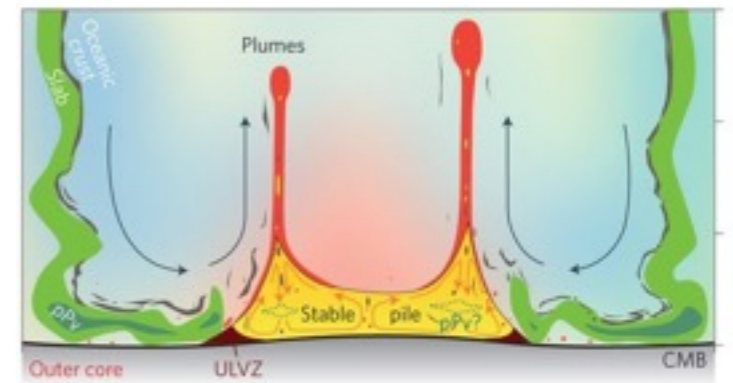
Melting and phase relations of deep mantle materials

$$T_{\text{CMB}} \sim T_{\text{solidus}}$$



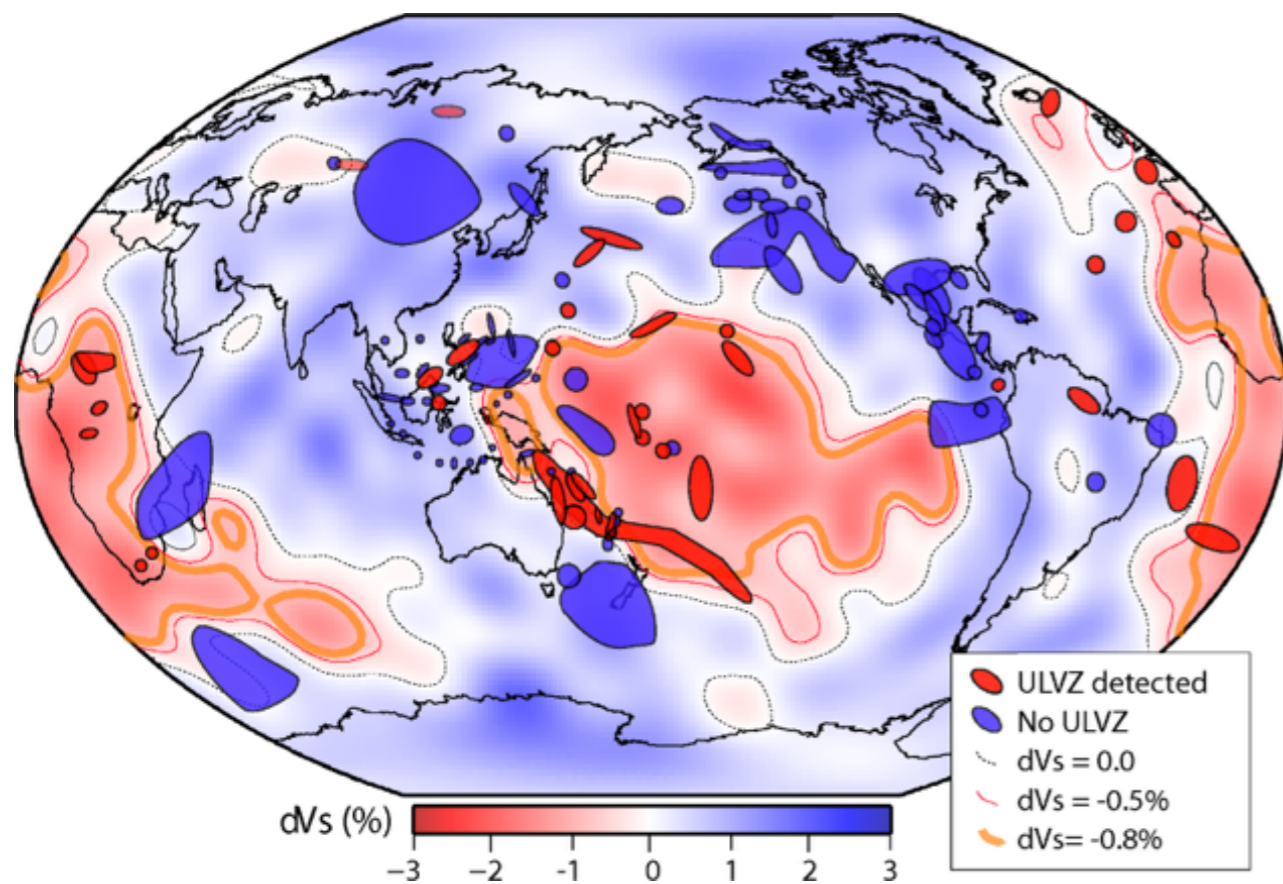
Concluding remarks

Nuclear resonant scattering techniques provide strong constraints on the vibrational thermodynamics (NRIXS), electronic environment (SMS), and melting (SMS) of Earth and planetary materials under extreme conditions.



ULVZs along the margins of thermochemical piles are likely compositional in origin.

- The **shear wave velocity** and density of magnesiowüstites permit a self-consistent model to explain these geophysically observed features.



(McNamara et al. EPSL 2010)

Further constraints on the **spin state** of candidate materials from SMS provides additional insights to the buoyancy of lower mantle assemblages.

The **melting curve** of $\text{Fe}_{0.9}\text{Ni}_{0.1}$ constrained by SMS, combined with plausible melting depressions, place CMB temperatures barely at or below the melting point of most deep Earth materials.

Thank you!